A correlation for the laminar burning velocity for use in hydrogen spark ignition engine simulation

Verhelst, Sebastian; T'Joen, Christophe; Vancoillie, Jeroen; Demuynck, Joachim

In: INTERNATIONAL JOURNAL OF HYDROGEN ENERGY, 36 (1), 957-974, 2011

http://dx.doi.org/10.1016/j.ijhydene.2010.10.020

A correlation for the laminar burning velocity for use in hydrogen spark ignition engine simulation

S. Verhelst[a]*, C. T'Joen[a,b], J. Vancoillie[a] and J. Demuynck[a]

[a]: Ghent University; Department of Flow, Heat and Combustion Mechanics; Sint-Pietersnieuwstraat 41, B-9000 Gent, Belgium

[b]: Delft University of Technology; Department of Radiation, Radionuclides & Reactors, Mekelweg 15, 2629 JB Delft, The Netherlands (current working address)

*corresponding author: T +32 9 264 3306; F +32 9 264 3590; E-mail Sebastian.Verhelst@UGent.be

Abstract

Hydrogen is an interesting fuel for internal combustion engines. It is a versatile fuel that enables high efficiencies and low emissions of oxides of nitrogen (NO_x), throughout the load range.

Computer simulations of hydrogen-fuelled spark ignition engines would facilitate the development of these engines. These necessitate the calculation of the turbulent combustion of hydrogen to track the flame propagation throughout the combustion chamber and resolve in-cylinder pressure and temperature. In order to do this, the laminar burning velocity of the in-cylinder mixture at the instantaneous pressure and temperature is needed. However, there is a scarcity of data in the literature, particularly at engine conditions. This is further complicated by the occurrence of flame instabilities at engine-like pressures, which compromises some of the existing data.

This paper discusses the available experimental data and correlations for the laminar burning velocity of hydrogen mixtures, and their deficiencies. One-dimensional chemical kinetic calculations of the laminar burning velocity of mixtures of hydrogen, air and residuals, at engine-like pressures and temperatures are then reported. A correlation is derived for use in hydrogen engine codes and is compared to other correlations presented previously.

Nomenclature

Greek Symbols

α	-	temperature exponent
β	-	pressure exponent
γ	-	residual gas coefficient
λ	-	air-to-fuel equivalence ratio

Symbols

k	1/s	rate of flame stretch
$D_{M,exc}$	cm²/s	mass diffusivity of the excess reactant
$D_{M,lim}$	cm²/s	mass diffusivity of the deficient reactant
D_T	cm²/s	thermal diffusivity of the unburned mixture
f	vol%	residual gas content
L	mm	Markstein length
Le	-	Lewis number
p	bar	pressure
T	K	temperature
u_l	cm/s	(stretch-free) laminar burning velocity
u_n	cm/s	stretched normal burning velocity

Abbreviations

CFD	computational fluid dynamics
DI	direct injection
EGR	exhaust gas recirculation
H_2ICE	hydrogen internal combustion engine
ICE	internal combustion engine
NO_x	oxides of nitrogen
NTP	normal temperature and pressure
SSD	sum of the squared differences

1. Introduction

As fossil fuel reserves are decreasing and emissions of noxious substances and greenhouse gases from the energy and transportation sector keep increasing, hydrogen becomes ever more interesting. If produced using renewable energy, it is an energy carrier with large potential [1, 2]. The internal combustion engine (ICE), used exclusively for road transport today, can be converted to hydrogen use [3-7]. Because of its wide flammability limits in air and large tolerance for exhaust gas recirculation (EGR), hydrogen can be burned in engines with high efficiencies and low emissions of NO_x (the only noxious component to be considered for hydrogen ICEs). A wide range of equivalence ratios is typically used, with considerable EGR concentrations, to maximize efficiency for all load demands.

The development of hydrogen fuelled ICEs (H2ICEs) would be greatly facilitated if accurate simulation tools were available, that can be used to optimize engines taking the properties of hydrogen into account. Recently, several hydrogen engine models have been reported, ranging from multi-zone thermodynamic engine models [8-10] to computational fluid dynamics (CFD) models [11-14]. All of these works stress the importance of accurate data on the laminar burning rate of mixtures of hydrogen, air and residuals from combustion (exhaust gas, internally or externally recirculated).

In order to allow computation of hydrogen combustion in engines as well as to increase the understanding of hydrogen combustion at engine conditions, data on the laminar burning velocity of hydrogen mixtures are needed, for a wide range of conditions. However, as demonstrated in the following section, such data are scarce or non-existing, or unusable.

This paper reviews the available data on hydrogen laminar burning velocity, highlights issues with the previously reported data and correlations, and reports calculations of the laminar burning velocity of hydrogen-air-residuals mixtures. A tentative correlation is presented as a function of equivalence ratio, pressure, temperature and residual gas fraction, that can be used in a hydrogen engine simulation code.

2. The laminar burning velocity and flame front instabilities

The laminar burning velocity of hydrogen mixtures and its dependence on mixture conditions and flame front instabilities have been discussed at length by one of the authors elsewhere [3]. For clarity, some of the discussion is repeated in the following sections, and now includes the most recent relevant literature.

The laminar burning velocity, u_l, of a fuel-air mixture is an important physicochemical property due to its dependence on pressure, temperature, mixture equivalence ratio and diluent concentration. It affects the combustion rate in an engine, the equivalence ratio limits for stable combustion, the

tolerance for EGR etc. Most engine combustion models assume the flame structure to be that of a (stretched) laminar flame, with the effect of the in-cylinder turbulence to stretch and to wrinkle the flame, thereby increasing the flame area. Consequently, data on the laminar burning velocity and its dependence on pressure, temperature, mixture composition and stretch rate are a prerequisite.
Several mechanisms exist that can trigger instability of a laminar flame. The discontinuity of density (with the unburned gas density being a multiple of the burned gas density) causes a hydrodynamic instability known as the Darrieus-Landau instability [15,16]. A flame is unconditionally unstable when only considering hydrodynamic stretch and neglecting the effect of flame stretch (see below) on the structure of the flame. The lower density of the burned gases compared to the unburned gases is also the cause for a second instability arising from gravitational effects. This body-force or buoyant instability, also known as the Rayleigh-Taylor instability, arises when a less-dense fluid is present beneath a more-dense fluid; such is the case in, e.g., an upwardly propagating flame. Finally, flame instability can be caused through unequal diffusivities [15,16]. Three diffusivities are of importance: the thermal diffusivity of the unburned mixture, D_T, the mass diffusivity of the deficient reactant (this refers to the reactant limiting the rate of reaction, thus, in a lean flame, the deficient reactant is the fuel), $D_{M,lim}$, and the mass diffusivity of the excess reactant, $D_{M,exc}$. The ratio of two diffusivities can be used to judge the stability of a flame when subjected to a perturbation or flame stretch. The Lewis number, Le, of the deficient reactant is defined as the ratio of the thermal diffusivity of the unburned mixture to the mass diffusivity of the deficient reactant: $Le=D_T/D_{M,lim}$. If this Lewis number is greater than unity, the thermal diffusivity exceeds the mass diffusivity of the limiting reactant. When this is the case, a wrinkled flame front will have parts that are “bulging” towards the unburned gases lose heat more rapidly than diffusing reactants can compensate for. The parts that recede in the burned gases, on the contrary, will increase in temperature more rapidly than being depleted of reactants. As a result, the flame speed of the “crests” will decrease and the flame speed of the “troughs” will increase, which counteracts the wrinkling and promotes a smooth flame front. The mixture is then called thermo-diffusively stable. When the Lewis number is smaller than unity, similar reasoning shows that a perturbation is amplified, which indicates unstable behavior. In the case of hydrogen, because of its very high mass diffusivity, for lean mixtures the Lewis number is much lower than unity (of the order of 0.3).
Another mechanism involving unequal diffusivities is the following: when the limiting reactant diffuses more rapidly than the excess reactant, $D_{M,lim}>D_{M,exc}$, it will reach a bulge of the flame front into the unburned gases more quickly and cause a local shift in mixture ratio. As in this case, the more diffusive reactant is the limiting reactant, the local mixture ratio will shift so that it is nearer to stoichiometry, and the local flame speed will increase. Thus, a perturbation is amplified and the resulting instability is termed a preferential diffusion instability. This mechanism is easily illustrated

by the propensity of lean mixtures with lighter-than-air fuels such as hydrogen to develop cellular flame fronts [17,18].

In reality, all mechanisms described above are simultaneously present. Disturbances of a flame front causing it to deviate from a steady planar flame can be summarized in one scalar parameter, the rate of flame stretch, , which is defined as the normalized rate of change of an infinitesimal area element of the flame,

(1)

The combined effect of the instability mechanisms is dependent on the magnitude of the stretch rate. For instance, thermo-diffusively stable spherically expanding flames start out smooth, as the stretch rate is initially high enough for thermo-diffusion to stabilize the flame against hydrodynamic instability. For small to moderate rates of stretch, the effect of stretch on the burning velocity can be expressed to first order [15] by:

(2)

where the subscript "n" denotes the stretched value of the normal burning velocity, and L is a Markstein length. Depending on the sign of L and whether the flame is positively or negatively stretched, the actual burning velocity can be increased or decreased compared to the stretch-free burning velocity, u_l. A positive Markstein length indicates a diffusionally stable flame, as flame stretch decreases the burning velocity. Any disturbances (wrinkles) of the flame front will thus tend to be smoothed out. A negative Markstein length indicates an unstable flame. A perturbation of the flame front will then be enhanced, and such flames quickly develop into cellular structures (see below for an example). Thus, when measuring burning velocities, it is important that this is done at a well-defined stretch rate and the Markstein length is simultaneously measured so that the stretch-free burning velocity can be calculated (which even some recent papers have failed to do [19]). It has taken a while for the effects of stretch to be understood and for measuring methodologies to be developed that could take the effects into account. As illustrated in the following section, this is the main reason for the large spread in the reported data on hydrogen mixture burning velocities throughout the years.

3. Literature review of available experimental data

Contemporary reviews of data and correlations for the laminar burning velocity of hydrogen-air mixtures show a wide spread of experimental and numerical results [3,20,21]. Figure 1 plots laminar burning velocities against the equivalence ratio for hydrogen-air mixtures at normal temperature and pressure (NTP). Note the large difference in burning velocities, with stoichiometric burning velocities

varying from 2.1 m/s up to 2.5 m/s, with even larger differences for the lean mixtures (e.g., for λ=2 from 56 cm/s to 115 cm/s, with λ the air-to-fuel equivalence ratio). The cause of this large spread can be found in the influence of the flame stretch rate on experimentally observed burning velocities. The filled symbols in Fig. 1 denote stretch-free burning velocities, as determined by Taylor [22], Vagelopoulos et al. [23], Kwon and Faeth [24] and Verhelst et al. [25]. These burning velocities were corrected to account for the effects of the flame stretch rate, using Eq. (2) (note that recent work points out that the extrapolation using Eq. (2) is only valid under certain conditions, which might not have been respected by these works [26,27]). The open symbols denote other measurements that did not take stretch rate effects into account, as reported by Liu and MacFarlane [28], Milton and Keck [29], Iijima and Takeno [30] and Koroll et al. [31]. These experiments result in consistently higher burning velocities, with the difference increasing for leaner mixtures. As explained in the previous section, the flame stretch rate can cause an increase in burning velocity or flame acceleration due to cellularity.

There are very few data available at engine conditions. The range of conditions covered by the correlations of Liu and MacFarlane [28], Milton and Keck [29], Iijima and Takeno [30] and Koroll et al. [31], mentioned above, include lean to rich mixtures and elevated temperatures (up to 550 K) and pressures (up to 25 atm). However, as discussed previously, they did not account for the effects of stretch and instabilities, which grow stronger with pressure as the flame thickness decreases [25]. Consequently, at engine-like pressures, the flame is cellular from inception onwards, accelerating throughout its growth, as illustrated in Fig. 2. The flame speed increases faster than linearly with decreasing flame stretch rate, consequently the methodology of obtaining stretch-free burning velocities u_l (and its dependence on stretch rate), using eq. (2), is no longer applicable [25,32].

To study the influence of temperature, pressure and residual gas content, Verhelst et al. [21,25] determined the burning velocity of a spherically expanding flame at a flame radius of 10 mm, for $1 \leq \lambda \leq 3.3$, $300\ K \leq T \leq 430\ K$, $1\ bar \leq p \leq 10\ bar$ and $0\ \% \leq f \leq 30\ \%$ (with T the temperature, p the pressure and f the residual gas content, in vol%). This burning velocity is not a fundamental parameter but, as the authors claim, “is indicative of the burning rate at a fixed, repeatable condition, representing a compromise that involves a sufficiently large radius to minimize the effects of the spark ignition, while being small enough to limit the acceleration due to the instabilities”. It is noteworthy that these are the only data that include the effects of residual gas content, an important parameter, given the operating strategies that are proposed for H_2ICEs.

An alternative methodology has been proposed to obtain u_l and Markstein lengths at higher pressures, from high speed schlieren photography of freely expanding spherical flames. The laminar burning velocity u_l as well as Markstein lengths have been reported for equivalence ratios from λ=3.3

up to stoichiometric, for pressures of 1, 5 and 10 bar [32]. However, this involved numerous experiments and very high camera frame rates. Furthermore, experimental uncertainty is rather high, especially on the Markstein lengths.

The most recent attempt at measuring laminar flame speeds with the goal of deriving a correlation for use in an engine code is reported by Gerke et al. [33]. They extensively discuss the effects of flame instabilities and demonstrate the resulting complexity of experimentally determining burning velocities, through measurements of propagating flames in a rapid compression machine. They measured flame speeds using OH-chemiluminescence as well as deriving flame speeds from the pressure rise, for a fairly large range of conditions ($0.4 \leq \lambda \leq 2.8$, $350\ K \leq T \leq 700\ K$, $5\ bar \leq p \leq 45\ bar$). The large variability, large error bars and large deviation between optical (OH) and thermodynamic (pressure) results clearly illustrate the problems in obtaining hydrogen flame speeds at engine conditions.

An alternative to the experimental determination is the use of a one-dimensional chemical kinetics code to calculate u_l. The H_2/O_2 system is one of the simplest reaction mechanisms, it is fairly well known (with more than 100 mechanisms reported in the literature, e.g., [34]) and computations of u_l are reasonably fast. However, it is perhaps surprising to learn that even for this simple system, there still exists a number of uncertainties, as recently reviewed by Konnov [35].

4. Literature review of chemical kinetic calculations

As the previous section has demonstrated, experimental determination of laminar burning velocities is difficult at engine-like conditions because of the occurrence of flame instabilities. Computationally, flame instabilities can be avoided by the assumption of a one-dimensional, planar flame. With this assumption, the accuracy of the calculated burning velocities depends on the accuracy of the molecular transport coefficients, the realism of the chemical kinetic reaction scheme, and the accuracy of the rate constants.

Several works report results for the laminar burning velocity of hydrogen mixtures calculated with one-dimensional chemical kinetics. Verhelst et al. report results comparing several published reaction mechanisms [21,36]. First, based on initial results the reaction mechanism of Ó Conaire et al. [37] was chosen as it resulted in the best correspondence with the selected experimental data at atmospheric conditions. Secondly, calculation results were compared with the experimental results from Verhelst et al. [21,25] for a range of pressures, temperatures, equivalence ratios and residual gas fractions. Note that these experimental results are not stretch-free burning velocities (see above). The authors report that the calculations break down for (very) lean mixtures and higher pressures. For moderately lean to stoichiometric mixtures, the effect of temperature and dilution

with residuals is reported to be predicted reasonably well. The inability of steady, planar calculations to predict burning velocities at very lean mixtures which are in agreement with experimentally observed values has recently been elucidated by Williams and Grcar [38], who demonstrate both through asymptotic analysis as through direct numerical simulation, that a premixed flame front can indeed propagate when the mixture is leaner than the flammability limit for planar flames. They provide evidence that this is due to the high diffusivity of molecular hydrogen, leading to a propagation mechanism that can be qualitatively seen as the advancement of a collection of point sinks of fuel into the fresh mixture. Thus, the high fuel diffusivity leads to a stratification with locally fuel- enriched zones.

Bradley et al. [32] compare their stretch-free experimentally determined data of u_l, at 5 and 10 bar, to calculations using the reaction mechanisms of Ó Conaire et al. [37] and Konnov [39]. The results using Konnov's scheme are reported to correspond best to the experimental results within the rather large uncertainty bands.

CFD simulations have been used by a team from TU Graz and BMW to investigate the mixture formation and combustion in DI engines [12-14]. The Fluent code was used with the turbulent burning velocity model by Zimont [40]. The laminar burning velocity was obtained from chemical kinetic calculations using the reaction scheme of Ó Conaire et al. [37], neglecting the influence of residual gas. The prediction of the flame propagation and rate of heat release corresponded well with measurements obtained in an optical engine.

Finally, Gerke et al. [33] also report burning velocity calculations using the scheme of Ó Conaire et al. [37], and compare them to the experimental results discussed in the previous section. Both their measured unstable burning velocities as the “stable” burning velocities derived from linear stability theory are higher than the values computed with the chemical kinetic scheme.

However, as the previous section has shown, experimental stretch-free data are scarce, especially at engine-like conditions. Thus, one has to keep in mind that validation of reaction mechanisms is very limited at best. Accurate burning velocity measurements at lean conditions are next to impossible because of instability. An alternative approach is to test reaction mechanisms on the basis of measured autoignition times [41,42].

5. Review of published correlations

A number of u_l correlations have been used in the literature for hydrogen engine cycle calculations. Using correlations is mostly preferred to using tabulated u_l data as they are more easily implemented in engine codes. Most correlations use the following form to express the influence of equivalence

ratio, pressure, temperature and residual gas content, as originally proposed by Metghalchi and Keck [43]:

— — (3)

This form is computationally convenient but assumes the effects of λ, p, T and f to be independent. In some cases, the exponents α, β or γ are expressed as a function of λ for a better fit to experimental data. A correlation of this form was derived for hydrogen mixtures from the experimental data reported by Verhelst et al. [21,25] and partly validated using an engine code [8]. Knop et al. [11] also proposed a correlation of this form, based largely on the correlation of Verhelst but extended to $\lambda<1$ (presumably through chemical kinetic calculations but not detailed in the paper) to allow computations of stratified combustion in DI engines (with locally rich mixtures). The comparison between simulated and measured engine cycles reported in the paper represents a limited validation of the correlation. Gerke et al. [33] also use Eq. (3), and present a correlation both for their measured pressure-derived burning velocities as for the computed burning velocities using a chemical kinetic mechanism. The effects of equivalence ratio are incorporated both in the u_{l0} term as through a λ dependence of the exponents α and β. For the residual gas term they refer to Verhelst [21].

However, Verhelst and Sierens [20] point out that in reality there can be a strong interaction between the effects of e.g. equivalence ratio and pressure, leading them to propose an alternative formulation for a laminar burning velocity correlation:

— (4)

Here, $u_{l0}(\lambda,p)$, $\alpha(\lambda,p)$, $\gamma_0(\lambda,p)$ and $\gamma_1(\lambda,p)$ are functions of the form:

(5)

This correlation involves more calculation steps than eq. (3) but is still easily implemented. D'Errico et al. [9,44] subsequently used this formulation to construct a correlation for the laminar burning velocity from chemical kinetic calculations using an in-house reaction scheme [45]. The correlation is claimed to be valid in the range $1 \le \lambda \le 2.8$, 500 K ≤ T ≤ 900 K, 1 bar ≤ p ≤ 60 bar. The validity range for is not stated in the paper. The authors use the correlation in full-cycle simulations using 1D gas dynamic calculations combined with a quasi-dimensional combustion model, for a hydrogen engine with cryogenic port injection. Engine cycle simulations were run for varying engine speed and equivalence ratio and compared to experiments. The combustion pressure was well predicted for stoichiometric and moderately lean mixtures, but was less satisfactory for

(very) lean conditions at medium to high engine speeds. The authors pointed to the effects of differential diffusion and instabilities for these (very lean) conditions and the high ratios of turbulent to laminar burning velocities reported for these mixtures [46], which were unaccounted for in the combustion model.

Although both formulations of a correlation for hydrogen mixtures have been partly validated through engine simulations, close inspection reveals a problem with the terms describing the effect of the residual gas fraction:

(6)

The term proposed by Verhelst et al. [21,25] and used in engine cycle simulation [8,11,47] uses a coefficient γ that is function of the equivalence ratio:

(7)

Thus, eq. (6) becomes negative for a certain residual gas fraction, depending on equivalence ratio. For example, for stoichiometric mixtures, a negative is obtained if exceeds 45vol%. However, hydrogen engine experiments have been reported with external EGR rates of 45% and higher [48,49], with normal combustion. If such operating strategies are to be simulated, it is clear that the residual gas terms, eqs. (6) and (7), are inadequate.

The alternative term from eq. (4), proposed by Verhelst et al. [20] and also used in engine cycle simulation [9,43], uses a coefficient that is function of the equivalence ratio, pressure and temperature:

(8)

Equation (8) implicates a higher tolerance for dilution with increased temperature (decreases with T, thus decreasing the result of eq. (6)). Verhelst et al. [20] gave coefficients for the and functions (see eq. (5)), valid in the range $1 \leq \lambda \leq 3$, $300\ K \leq T \leq 800\ K$, $1\ bar \leq p \leq 16\ bar$. For stoichiometric mixtures the residual gas term also becomes negative if exceeds 45vol%. D'Errico et al. [9,44] use the same coefficients for the and functions but, as stated above, claim them to be valid in the range $1 \leq \lambda \leq 2.8$, $500\ K \leq T \leq 900\ K$, $1\ bar \leq p \leq 60\ bar$. However, such an extrapolation to much higher pressures leads to non-physical results: depending on the temperature, the residual gas term can even become greater than 1, implying that diluting the mixture with residual gas would increase the burning velocity, which clearly is not the case (see also Section 6.4). Also, ref. [9] gives the same coefficients as ref. [20] although the correlation form for and uses the fuel-to-air equivalence ratio ϕ in [9], as opposed to λ in ref. [20]. Finally, ref. [9] states that is the mass fraction of residual gases, whereas it is defined as a volume fraction in ref. [20].

In order to allow computation of the laminar burning velocity of hydrogen mixtures at the conditions that are currently explored in hydrogen engine operating strategies, one-dimensional chemical kinetic calculations are reported here, the results of which are then fitted to a new correlation form.

6. Calculations and correlation

6.1. Choice of kinetic scheme and range of conditions

Based on the studies discussed in Section 4, the reaction scheme of Konnov [39] was chosen for the calculation of the laminar burning velocity of hydrogen mixtures, as it is the only scheme (partly) validated at elevated pressures, using stable burning velocities [32]. The Chem1D one-dimensional chemical kinetics code developed at the Technical University of Eindhoven [50] was used to calculate a one-dimensional planar adiabatic flame, the burning velocity of which is by definition. Calculations have been performed for , , and . This range covers most of the expected conditions that the unburned mixture in a hydrogen-fuelled engine will experience. Over 1000 conditions within this range have been calculated to build up a database to which a correlation can be fitted (see below). The parameter range is clarified in Table 1.

6.2. Laminar burning velocity without residual gases

In order to determine the correlation the dataset was first examined in more detail to determine the effect of the different parameters on the laminar burning velocity values. A reference temperature and pressure were defined (p_0 = 1 bar, T_0 = 300 K) and used to make the pressure and temperature non-dimensional. The initial analysis combined with the literature survey suggested the following functional form for the correlation (Eq. (9)-(10)):

$$u_l(\lambda, p, T, f) = u_{l0}(\lambda, p)\left(\frac{T}{T_0}\right)^{\alpha(\lambda,p)} F(\lambda, p, T, f) \qquad (9)$$

$$F(\lambda, p, T, f) = 1,\ f = 0 \qquad F(\lambda, p, T, f) < 1,\ f > 0 \qquad (10)$$

This form is based on the earlier correlation of Verhelst and Sierens [20], see Eq. (4), but with a different correction term F to account for the impact of residual gases. Figure 3 shows the natural logarithm of u_l set out against the natural logarithm of T/T_0 for a number of data series without residual gases. This figure clearly supports the proposed power relationship as all the data series are almost perfectly linear. This was the case for all considered data points (f = 0). So for each combination of pressure and equivalence ratio the intercept (ln u_{l0}) and the slope (α) of the linear

relation were determined. This resulted in 30 values which were then fit as a function of p/p_0 and λ. As noted by Verhelst and Sierens [20] both $\alpha(\lambda, p)$ and $u_{l0}(\lambda, p)$ are a complex function of p and λ due to the strong interaction between these variables.

The Levenberg-Marquadt algorithm [51] was used to determine the coefficients of the fitted equations. This algorithm seeks to reduce the sum of the squared differences (SSD) between the observed and predicted values. Due to the large spread in u_l values (ranging from cm/s to more than 14 m/s) a weighting parameter was used during the fitting, to ensure an accurate fit also for the lower burning velocities. The weighting was set to the squared reciprocal of the observed value as this gave the best results (this roughly corresponds to minimizing the relative differences between observed and predicted values). Each of the proposed equations (see below, Eqs. 11 – 12 – 18) in this paper is the result of a large number of iterations, whereby different functional forms were fit to the data. Initially these forms consisted of only linear terms in the different variables (p/p_0, λ, f, T/T_0). Progressively terms were added, first 'pure' quadratic terms ($(p/p_0)^2$, λ^2, f^2, $(T/T_0)^2$) followed by linear cross terms (e.g. (p/p_0) x t, t x f…), inverse linear terms (e.g. $1/(p/p_0)$) and progressively higher order terms and combinations of these factors. This was continued until the resulting SSD no longer decreased. Once this stage was reached it was attempted to 'trim' the equation, by selectively removing terms one by one to see their impact on the SSD. Usually a number of terms could be removed at this stage, as their impact on the prediction of u_l was covered by a cross term. Once such a relationship was found, the process was repeated but with a different order in which the cross terms and higher order terms were added to the fit. Eventually the equation which resulted in the smallest SSD is presented here.

All of the proposed relationships are valid within the entire considered parameter range. Even though it is possible to reduce the SSD further by splitting the database up into smaller parts (e.g. lean and rich mixtures), this makes the correlations less generally applicable and presents problems at the boundaries where they should overlap. It was therefore preferred to present equations which are valid over the entire range.

Table 2 lists the coefficients to determine $\alpha(\lambda, p)$ using Eq. (11).

$$\alpha(\lambda, p) = a_1 + a_2\lambda + a_3\frac{p}{p_0} + a_4\frac{p}{p_0}\lambda + a_5\lambda^2 + a_6\left(\frac{p}{p_0}\right)^2 + a_7\lambda^2\frac{p}{p_0} + a_8\lambda\left(\frac{p}{p_0}\right)^2 + a_9\lambda^2\left(\frac{p}{p_0}\right)^2 + \frac{a_{10}}{\lambda} + a_{11}\frac{p}{p_0}\frac{1}{\lambda} \quad (11)$$

Initially it was attempted to fit u_{l0} (determined by taking the exponential of the intercept value, see Fig. 3) to λ and p/p_0. However, due to the large variation in these values, it required an extensive amount of higher order terms (which makes sense as it was a polynomial approximation of an exponential relationship). Thus, in order to reduce the complexity of the fit, the intercept value itself, $\ln u_{l0}$, was fit instead. Table 3 lists the coefficients to determine $\ln u_{l0}(\lambda, p)$ using Eq. (12).

$$\ln u_{l0}(\lambda, p) = b_1 + b_2\lambda + b_3\frac{p}{p_0} + b_4\frac{p}{p_0}\lambda + b_5\lambda^2 + b_6\left(\frac{p}{p_0}\right)^2 + b_7\lambda^2\frac{p}{p_0} + b_8\lambda\left(\frac{p}{p_0}\right)^2 + b_9\lambda^3\frac{p}{p_0} + b_{10}\lambda\left(\frac{p}{p_0}\right)^3 + b_{11}\lambda^2\left(\frac{p}{p_0}\right)^2 + \frac{b_{12}}{\lambda} + b_{13}\frac{p}{p_0}\frac{1}{\lambda} \quad (12)$$

Figure 4 compares the predicted u_l values (using Eq. 13), note this is without the correction term F) to the dataset for all the fitted data points (149 in total). Not all the data points were used: the data for λ = 0.775 was kept as test data. The ±10% and ±20% prediction ranges are added in the figure.

$$u_{l,pred}(\lambda, p, T) = u_{l0}(\lambda, p)\left(\frac{T}{T_0}\right)^{\alpha(\lambda,p)} \quad (13)$$

Column 1 of Table 4 provides an overview of the quality of this fit, listing the average relative residual (Eq. (14)), average absolute relative residual (Eq. (15)), maximum and minimum residual and the percentage of the data points which is predicted to within ±10% and ±20%. As can be seen, the fit captures 97% of the data to within ± 20% and has a mean absolute residual of 5.65%.

$$\text{Average relative residual} = \frac{1}{N}\sum\left(\frac{u_{l,pred} - u_l}{u_l}\right) \quad (14)$$

$$\text{Average absolute relative residual} = \frac{1}{N}\sum\left(\frac{\left|u_{l,pred} - u_l\right|}{u_l}\right) \quad (15)$$

Figure 5 shows a comparison of the predicted u_l values (through Eq. (13)) for the test data. The resulting fit statistics are listed in Table 4. The test data consisted out of 3 batches. The first one was data which were discarded in the fitting process (λ = 0.775), the second one consisted of additional points generated for a higher temperature (1000K), and the third and major batch was formed by interpolation data based on the fitted dataset. This last batch of data was generated for p (10, 20, 30 and 40 bar), T (550 K, 650 K, 750 K and 850 K) and λ (0.3, 1.5 and 2.5). These interpolations were done separately for each parameter to avoid extrapolating the data too much; so e.g. the pressure interpolation is based on temperature and equivalence ratio data which is part of the dataset. The interpolation was done using curve fits which resulted in smooth behaviour between the data points

(this was visually verified). Different curves were used, selected after being tested to ensure the same curve can be used for the entire parameter range. For the temperature fit an exponential curve was used (Eq. (16)).

$$u_{l,fit}(\phi, p, T_{fit}, f) = y_0 + ae^{bT} \quad (16)$$

For the pressure a linear-exponential combination (Eq. (17)) was used.

$$u_{l,fit}(\phi, p_{fit}, T, f) = y_0 + ae^{-bp} + cp + \frac{d}{p} \quad (17)$$

For the equivalence ratio a more elaborate fit was needed, whereby first α and $\ln(u_0)$ were fit using the exponential linear relationship. These values were then used to compute the test data. Some examples are shown in Fig. 6 for the temperature (A) and pressure (B), with the filled symbols corresponding to database values and open symbols to generated test values. This resulted in a database of 425 test points. Figure 5 compares the predicted u_l values (through Eq. (13)) to the test data. The proposed relationship captures 99% of the test data to within ± 20% and has a mean absolute residual of 4.78 %. Note how the correlation spans a very large range (from a few cm/s up to 25 m/s) but is able to provide satisfactory accuracy over the entire range.

6.3. Correction term to account for residual gases

Having first fit the laminar burning velocity for the cases with no residual gases, the correction term describing the influence and interaction of the pressure, temperature, equivalence ratio and the volume fraction of the residual gases on the u_l values now has to be determined. Verhelst and Sierens [20] previously suggested a linear relationship in T and f combined with quadratic terms in p and λ. For low pressure and equivalence ratio, the trend in T/T_0 is indeed linear, but as pressure or equivalence ratio increases, the trend becomes quadratic. This is indicated in Fig. 7. This figure shows a number of data series for the correction term (computed as the ratio of the dataset values, with residuals, to the corresponding predicted values, without residuals, using the correlation proposed above, Eqs. (11)-(13)) set out against temperature, for stoichiometric mixtures (λ=1). Just as for the data without residual gases a strong coupling between p and λ was found in the correction term, including higher order terms. Of the different parameters, f has the strongest impact on the value of the correction term: increasing the residual gas content from 0 to 50 vol % results in a decrease of F from 1 to about 0. Instead of percentage values (e.g. 20%), decimal values (0.2) are used in all computations.

Using a similar procedure as described above a functional form was determined for the correction term, minimizing the SSD. During this fitting procedure we opted to remove the smallest values (< 10 cm/s) from the dataset. This was done because the required correction factor for these cases is often very small (0.02 and less) and as the squared reciprocal of this value is used as weighting factor the algorithm was unable to provide a satisfactory fit which covered the entire dataset. Furthermore the fitting was focused on the part of the dataset which is considered by the authors to be the most appropriate for engine simulations. The entire temperature range (500 to 900 K) was considered but for extreme λ values (< 0.55 and > 2) the highest concentrations of residual gases (f > 30%) were excluded. The considered dataset is highlighted in gray in Table 1. Table 5 lists the coefficients to determine $F_1(T, \lambda, p, f)$ using Eq. (18). The correction term $F(T, \lambda, p, f)$ is then found by limiting $F_1(T, \lambda, p, f)$ to be smaller than or equal to 1.

$$F_1(T, f, \lambda, p) = c_1 + c_2 \frac{T}{T_0} + c_3 \frac{p}{p_0} + c_4 \lambda + c_5 f + c_6 \left(\frac{p}{p_0}\right)^2 + c_7 \left(\frac{T}{T_0}\right)^2 + c_8 \lambda^2 + c_9 f^2 + c_{10} \frac{T}{T_0} \frac{p}{p_0} + c_{11} \frac{p}{p_0} \lambda + c_{12} f \lambda + \frac{c_{13}}{\lambda} + \frac{c_{14}}{\lambda} \frac{T}{T_0} + c_{15} \frac{p_0}{p} \frac{T}{T_0} + c_{16} \frac{T}{T_0} f^3 + c_{17} \frac{p}{p_0} f^3 + c_{18} \lambda f^3 + c_{19} \frac{p}{p_0} \frac{1}{\lambda} + c_{20} \frac{p}{p_0} f + c_{21} f \frac{T}{T_0} \quad (18)$$

$$F(T, f, \lambda, p) = \min(1, F_1(T, f, \lambda, p)) \quad (19)$$

Figure 8 compares the predicted u_l values to the dataset for all the fitted data points (781 in total). As can be seen almost all data points are within the ± 25% bounds, except at lower values where a small number of points lie just outside. It is true that compared to the case without residual gases the scatter is more pronounced in this fit, which is due to the strong impact of residual gas content on the laminar burning velocity. However, the fitting statistics indicate a good reliability of the fit, as shown in Table 4. 94.5% of the data points are predicted to within ± 25%. The mean absolute relative residual is 10.1 %. The large variation is mainly located at lower u_l values (< 250 cm/s) and at the edges of the fitted domain (500 or 900K and f = 0.5 for 0.55 ≤ λ ≤ 2, f = 0.1 for λ < 0.55 or f = 0.3 for λ = 3). At higher u_l values almost all of the data is within ± 10% (Fig. 8).

Similar to the previous fit, test data were generated from the database points. Interpolation was done for the pressure (10, 20, 30 and 40 bar), temperature (550 K, 650 K, 750 K and 850 K) and equivalence ratio (1.5 and 2.5, considering at lower values the grid is already quite fine, see Table 1). For the temperature interpolation the exponential form was used, Eq. (16). The exponential-linear combination, Eq. (17), was used for the pressure interpolation. As the data points for f were already closely spaced, it was selected not to add additional data points interpolating for f. This resulted in 1210 test points. The results are presented in Fig. 9 and the statistics can be found in Table 4. The

proposed relationship is able to predict 94% of the test data to within ± 25% and has a mean absolute relative residual of 9.3%. The same remarks apply here as for the earlier presented fitted data (Fig. 8), highlighting the overall quality of the fit, being able to well reproduce the high values (within ± 10%), and with the scatter mainly located at lower u_l values and towards the edges of the fitted domain.

Having determined the coefficients for the correction term F, the full correlation is now known. It consists of Eq. (9) whereby $\alpha(\lambda,p)$, $u_{l0}(\lambda,p)$ and $F(T, \lambda, p, f)$ are computed through Eqs. (11) – (12) – (18) – (19) respectively, making use of the coefficients listed in Tables 2, 3 and 5, with p_0 and T_0 as given above, f the volume fraction of residuals and u_l given in cm/s. Figure 10 presents the comparison of the predicted values to the database for all available points. The correlation predicts 96.2% of the database points within ±20% and has a mean absolute relative residual of 9.5%.

7. Comparison to other correlations

7.1. Statistical comparison

The correlation presented in the previous section was compared to the correlations published previously. The comparison includes:

- the present correlation, Eq. (9), making use of Eqs. (11) – (12) – (18) – (19)
- the correlation presented by Verhelst et al. [21,25] based on experimental data (not corrected for the effects of stretch and instabilities) , using the correlation form of Eq. (3), "Verhelst",
- the correlation presented by Knop et al. [11], based on a combination of the correlation by Verhelst et al. and chemical kinetic calculations, using the correlation form of Eq. (3), "IFP",
- the correlation presented by Gerke et al. [33], based on experimental data (not corrected for the effects of stretch and instabilities), using the correlation form of Eq. (3), "ETH exp",
- the correlation presented by Gerke et al. [33], based on chemical kinetic calculations using the mechanism of Ó Conaire et al. [37] , using the correlation form of Eq. (3), "ETH kin. corr.",
- the correlation presented by D'Errico et al. [9], based on chemical kinetic calculations using the mechanism of Frassoldati et al. [45] , using the correlation form of Eq. (4), "Milano".

As a basis for the comparison the results from the detailed kinetics calculations were used, because of the lack of experimental data as discussed earlier. It should be stressed that, as also treated above, the range of conditions calculated is out of the range of the proven reliability of chemical kinetic schemes. The calculations were limited to $\lambda \geq 1$ in the case of the correlations of Verhelst et al. and D'Errico et al., and limited to $\lambda < 3$ in the case of the two correlations of Gerke et al. and the correlation of D'Errico et al., to take the reported validity ranges into account.

First, a statistical analysis was made, analogous to the analysis that led to Table 4 using Eqs. (14) and (15). Table 6 lists the average relative residual (Eq. (14)), average absolute relative residual (Eq. (15)), maximum and minimum residual and the percentage of the results calculated using the different correlations which correspond to the detailed kinetics results to within ±10%, ±20% and ±25%. Figure 11 plots the burning velocities computed from the different correlations versus the burning velocities calculated with the one-dimensional chemical kinetics code, showing the ±10% and ±20% ranges.
It is clear from Table 6 and Fig. 11 that there are very large differences, between the results obtained from the previous correlations and from the present one, and between the previous correlations themselves. The correlation with the best correspondence to the kinetic results is "ETH kin. corr.", which is no surprise being itself a fit to detailed kinetics results within a similar range of conditions. However, "best correspondence" is a relative notion: looking at the statistics in Table 6 and confirmed visually from Fig. 11, the differences with the detailed kinetic results presented in this paper are substantial. This is even more the case for the "Verhelst" and "IFP" correlations, which can be seen to result in relatively similar values. Looking at the "ETH exp." correlation results, it is clear that they are consistently higher than the reference. Finally, using the "Milano" correlation leads to a wide spread in burning velocities, with some of them even negative. In the following paragraphs, the differences between the correlations are illustrated for a few selected conditions.

7.2. Graphical illustration

To provide a graphical illustration of the differences in behavior of the correlation presented here and in previous literature, 5 conditions were selected to compare the present correlation to previously reported correlations, first for cases without residual gases. As in engines, higher pressures will be accompanied by higher temperatures, the following conditions were selected from the database given in Table 1 (marked by the bold X's):

- (5 bar; 500 K)
- (15 bar; 600 K)
- (25 bar; 700 K)
- (35 bar; 800 K)
- (45 bar; 900 K)

A more conventional approach would be to illustrate the differences with graphs in which one parameter is varied while the others are kept constant, but in our opinion this has little practical relevance as that does not correspond to actual combinations of e.g. p and T. Thus, burning velocities were calculated for these, admittedly rather arbitrarily chosen, 5 conditions, at three equivalence ratios, also selected from the database: a rich condition (λ=0.55), a stoichiometric mixture (λ=1) and

a lean one (λ=2). The residual gas content was set to be zero for all cases (the correction term for residuals will be evaluated in the following section).

Figure 12 plots laminar burning velocities for the 5 conditions at the 3 equivalence ratios, calculated using the correlations listed above. The correlation presented in this paper is marked in the figure as "Eq. (13)", as the comparison is limited here to conditions without residuals. The values from the present database as calculated by Chem1D using Konnov's mechanism [39] are also shown. Although 5 discrete sets of conditions of pressure and temperature were selected for the comparison, the results from the correlations are shown using interconnected lines. This was done for clarity. The top graph of Fig. 12 (λ=0.55) does not show results for the correlations "Verhelst" and "Milano", as these correlations are only valid for $\lambda \geq 1$. In terms of pressure and temperature, the correlation "ETH exp" is used outside of its validity domain for some points (T>700 K).

As discussed in Section 3, there unfortunately is little or no accurate data for the laminar burning velocity of hydrogen mixtures at engine conditions, so Fig. 12 does not include experimentally measured data points. Thus, the correlations can only be compared qualitatively and judged by the trends they predict. Even so, some interesting observations can be made:

- First, the correlation based on cellular flames in a rapid compression machine ("ETH exp") predicts substantially higher velocities than all others.
- The correlation based on chemical kinetic calculations given by Gerke et al. ("ETH kin. Corr.") predicts the burning velocity at 15 bar and 600K to be the lowest of the 5 conditions, for the 3 equivalence ratios. For the other correlations, the lowest burning velocity is for the lowest temperature condition (5 bar, 500 K) at the rich and stoichiometric conditions. The correlation based on experimental results given by Gerke et al. ("ETH exp") also shows a "discontinuous" trace around the 15 bar, 600 K point, not seen with the other correlations.
- The results from the correlations fitted to chemical kinetic calculations using the mechanisms of Ó Conaire et al. and Konnov, "ETH kin. corr." and "Eq. (13)" respectively, are fairly close for the higher pressure and temperature points, especially for the lean case.
- At stoichiometry, the results using the correlations "Verhelst" and "IFP" are almost identical (the lines overlap in the figure), whereas a clear difference can be seen for the lean case.
- For the lean case, the correlation proposed by D'Errico et al. ("Milano") results in a completely different trend compared to the other correlations.
- Finally, it can be seen again that Eq. (13) gives results very close to the detailed results from the chemical kinetic calculations.

Based on these observations, and although not corroborated by experimental "evidence", it is safe to say that the correlations of D'Errico et al. ("Milano") and Gerke et al. ("ETH kin. corr.") seem to have

a smaller validity range than that claimed by these authors, probably due to the inadequate correlation form, being too simple to reproduce all the trends given by the detailed kinetic calculations.

Next, an assessment is made of the behavior of the correction term accounting for the effect of residual gases.

7.3. Graphical illustration of the correction term for residual gases

As the number of data points increases when also including the residual gas content as a variable, a reduced set of conditions was chosen for the illustrative comparison of the behavior of the residual gas correction term. First, as all previously reported correlations incorporate the effect of residuals either by Eq. (7) proposed by Verhelst et al. [25] or Eq. (8) proposed by Verhelst and Sierens [20], which are only valid in the stoichiometric to lean region, the comparison is limited to a stoichiometric (λ=1) and lean case (λ=2). Second, 3 conditions in pressure and temperature were chosen:

- (5 bar; 500 K)
- (25 bar; 700 K)
- (45 bar; 900 K)

The correction term representing the effect of residuals is then compared using:

- Equation (19), shown in the following graphs as “Eq. (19)”,
- Equation (7), shown as “Verhelst expt.”,
- Equation (8), shown as “Verhelst kin.”,
- As well as the correction term directly calculated from the detailed kinetic results, “detailed kinetics”.

Figure 13 shows the calculated correction term for stoichiometric mixtures, for a residual gas content going from 0 to 50 vol%. A distinction can be made between the linear trend obtained using Eqs. (7) and (8) (respectively “Verhelst expt.” and “Verhelst kin.”) and the quadratic trend obtained using Eq. (19) and from the detailed kinetics. It is clear that Eq. (7) (“Verhelst expt.”) predicts negative values when the residual gas content is higher than 45 vol%, as stated above. Equation (8) (“Verhelst kin.”) gives results close to Eq. (7) for the first two conditions (5 bar – 500 K and 25 bar – 700 K) but gives negative results at the 45 bar – 900 K condition for residual gas contents above 25 vol%. This is no surprise as the correlation is used far outside of its validity range [20] (although it is used in a wider range in ref. [9]). Results obtained with Eq. (19) are positive for all conditions and closely follow the detailed chemical kinetic calculations.

Figure 14 shows the correction term for lean, λ=2, mixtures. As stated above, for the leaner mixtures the calculated range for residual gas content is smaller, with values shown up to 30 vol% of residuals. Again, a distinction can be made between the linear behavior of the terms previously proposed by Verhelst et al., and the quadratic behavior of the detailed kinetic results and their fit (Eq. 19). Here, Eq. (8) ("Verhelst kin.") predicts an increase in the correction term (and thus an increasing burning velocity) with increasing residual gas content for the 45 bar – 900 K condition, which clearly is not physical. For these lean cases, Eq. (7) ("Verhelst expt.") results in higher values for the correction term than Eq. (19) (i.e. a smaller decrease of burning velocity in the presence of residuals).

Here, the new correlation for the effect of residuals is clearly superior to the previous formulations, being valid for a wider range of conditions (including rich mixtures) and always giving physically meaningful results.

8. Conclusion

This paper started by stressing the importance of accurate data for the laminar burning velocity of hydrogen mixtures, at pressures and temperatures such as occurring in internal combustion engines, and of data for the effect of residual gases. It has been shown that unfortunately, very few such data exist. Reasons for this have been discussed, namely the presence of flame stretch in most experimental setups, and the unstable nature of high pressure flames making experimental determination very difficult. As a consequence, the few data at engine conditions that can be found in literature, are either not "true" laminar burning velocities (i.e. stable and stretch-free) or are associated with large uncertainties. As previously concluded, further work to provide accurate experimental data remains of critical importance [3].

As no stable laminar flames will exist at engine conditions, it can be argued that laminar burning velocities, i.e. the burning velocities of stable planar flames, lose their validity as input for combustion models [32,33]. However, data for u_l at engine conditions are still relevant, be it to be able to assess the impact of instabilities, or to provide an unambiguous reference for e.g. measured or modeled turbulent burning velocities. Approaches have been shown in literature that use stability theory to compute burning velocities for stable flames, from measured data of unstable flame propagation [32,33]. Perhaps the inverse can be done to compute relevant unstable burning velocities from stable data for u_l. Such data can be generated using chemical kinetic calculations (it would also require the computation of Markstein lengths), although the validity of the used reaction

scheme is hard to assess precisely because of the lack of experimental data to validate to the scheme.

Thus, the present paper reports values for the laminar burning velocity of hydrogen mixtures, obtained from chemical kinetic calculations, using a reaction scheme that was at least partially validated against burning velocity measurements at increased temperature and pressure. This was done for a wide range of conditions representative of engine combustion: $0.2 \leq \lambda \leq 3.0$, $500\ K \leq T \leq 900\ K$, $5\ bar \leq p \leq 45\ bar$ and $0\ vol\% \leq f \leq 50\ vol\%$. A lot of attention was devoted to a suitable formulation of a correlation fitting these results, as such a correlation is more easily implemented in an engine code and allows a better comparison to existing correlations. Deficiencies of the correlations previously used in literature have been discussed, and a comprehensive study of the impact of the different parameters resulted in a new type of correlation closely fitting the detailed kinetic results. As the influence of residual gases was incorporated in a separate correction term, this can easily be added to other correlations.

Acknowledgements

The authors would like to thank Ronny Tuybens for contributing to this work during his MSc thesis, and the Combustion Technology section at the Technical University of Eindhoven, in particular Prof. Philip de Goey, Dr. Bart Somers and Dr. Jeroen Van Oijen, for the use of and help with the Chem1D code. J. Vancoillie acknowledges the Research Foundation - Flanders (FWO) for the PhD grant 09/ASP/030, J. Demuynck acknowledges the Institute for the Promotion of Innovation through Science and Technology in Flanders (IWT Vlaanderen) for the PhD grant SB-081139.

References

[1] Abbott D. Hydrogen Without Tears: Addressing the Global Energy Crisis via a Solar to Hydrogen Pathway, Proc. IEEE 2009;97:1931-4.

[2] Abbott D. Keeping the Energy Debate Clean: How Do We Supply the World's Energy Needs?, Proc. IEEE 2010;98:42-66.

[3] Verhelst S, Wallner T, Hydrogen-Fueled Internal Combustion Engines, Progress in Energy and Combustion Science 2009;35:490-527.

[4] Verhelst S, Maesschalck P, Rombaut N, Sierens R. Efficiency comparison between hydrogen and gasoline, on a bi-fuel hydrogen/gasoline engine, Int J Hydrogen Energy 2009;34:2504-10.

[5] Verhelst S, Maesschalck P, Rombaut N, Sierens R. Increasing the power output of hydrogen internal combustion engines by means of supercharging and exhaust gas recirculation, Int J Hydrogen Energy 2009;34:4406–12.
[6] Verhelst S, Verstraeten S, Sierens R. A critical review of experimental research on hydrogen fueled SI engines. SAE technical paper nr 2006-01-0430. Also in SAE Trans 2006 J Engines 264–74.
[7] White CM, Steeper R, Lutz AE. The hydrogen-fueled internal combustion engine: a technical review. Int J Hydrogen Energy 2006;31:1292–305.
[8] Verhelst S, Sierens R. A quasi-dimensional model for the power cycle of a hydrogen fuelled ICE. Int J Hydrogen Energy 2007;32:3545–54.
[9] D'Errico G, Onorati A, Ellgas S. 1d Thermo-fluid dynamic modelling of an SI single-cylinder H2 engine with cryogenic port injection. Int J Hydrogen Energy 2008;33:5829–41.
[10] Safari H, Jazayeri S, Ebrahimi R. Potentials of NOx emission reduction methods in SI hydrogen engines: simulation study. Int J Hydrogen Energy 2009;34:1015–25.
[11] Knop V, Benkenida A, Jay S, Colin O. Modelling of combustion and nitrogen oxide formation in hydrogen-fuelled internal combustion engines within a 3D CFD code. Int J Hydrogen Energy 2008;33:5083–97.
[12] Wimmer A, Wallner T, Ringler J, Gerbig F. H2-direct injection – a highly promising combustion concept. SAE Paper No. 2005-01-0108 (2005).
[13] Messner D, Wimmer A, Gerke U, Gerbig F. Application and validation of the 3D CFD method for a hydrogen fueled IC engine with internal mixture formation. SAE Paper No. 2006-01-0448 (2006).
[14] Gerke U, Boulouchos K, Wimmer A. Numerical analysis of the mixture formation and combustion process in a direct injected hydrogen internal combustion engine. Proceedings 1st international symposium on hydrogen internal combustion engines. pp. 94–106 (Graz, Austria, 2006).
[15] Clavin P. Dynamic behaviour of premixed flame fronts in laminar and turbulent flows. Prog Energy Combust Sci 1985;11:1–59.
[16] Williams FA. Combustion theory. 2nd ed. Addison-Wesley; 1985.
[17] Kwon S, Tseng LK, Faeth GM. Laminar burning velocities and transition to unstable flames in H2/O2/N2 and C3H8/O2/N2 mixtures. Combust Flame 1992;90:230–46.
[18] Hertzberg M. Selective diffusional demixing: occurrence and size of cellular flames. Prog Energy Combust Sci 1989;15:203–39.
[19] Ilbas M, Crayford AP, Yilmaz I, Bowen PJ, Syred N. Laminar-burning velocities of hydrogen-air and hydrogen-methane-air mixtures: an experimental study. Int J Hydrogen Energy 2006;31:1768-1779.
[20] Verhelst S, Sierens R. A laminar burning velocity correlation for hydrogen/air mixtures valid at spark-ignition engine conditions, ASME Spring Engine Technology Conference paper nr. ICES2003-555 (Salzburg, Austria, 2003).

[21] Verhelst S. A study of the combustion in hydrogen-fueled internal combustion engines. PhD thesis, Ghent University, Gent, Belgium; 2005. http://hdl.handle.net/1854/3378.
[22] Taylor SC. Burning velocity and the influence of flame stretch. PhD thesis, Leeds University, 1991.
[23] Vagelopoulos CM, Egolfopoulos FN, Law CK. Further considerations on the determination of laminar flame speeds with the counterflow twin-flame technique. 25th Symp. (Int.) on Combustion 1341–7, 1994.
[24] Kwon OC, Faeth GM. Flame/stretch interactions of premixed hydrogen-fueled flames: measurements and predictions. Combust Flame 2001;124:590–610.
[25] Verhelst S, Woolley R, Lawes M, Sierens R. Laminar and unstable burning velocities and Markstein lengths of hydrogen–air mixtures at engine-like conditions. Proc Combust Inst 2005;30:209–16.
[26] Pareja J, Burbano HJ, Ogami Y. Measurements of the laminar burning velocity of hydrogen-air premixed flames. Int J Hydrogen Energy 2010;35:1812-18.
[27] Chen Z, Burke MP, Ju Y. Effects of Lewis number and ignition energy on the determination of laminar flame speed using propagating spherical flames. Proc Combust Inst 2009;32(1):1253-60.
[28] Liu DDS, MacFarlane R. Laminar burning velocities of hydrogen–air and hydrogen–air–steam flames. Combust Flame 1983;49:59–71.
[29] Milton B, Keck J. Laminar burning velocities in stoichiometric hydrogen and hydrogen–hydrocarbon gas mixtures. Combust Flame 1984;58:13–22.
[30] Iijima T, Takeno T. Effects of temperature and pressure on burning velocity. Combust Flame 1986;65:35–43.
[31] Koroll GW, Kumar RK, Bowles EM. Burning velocities of hydrogen–air mixtures. Combust Flame 1993;94:330–40.
[32] Bradley D, Lawes M, Liu K, Verhelst S, Woolley R. Laminar burning velocities of lean hydrogen–air mixtures at pressures up to 1.0 MPa. Combust Flame 2007;149:162–72.
[33] Gerke U, Steurs K, Rebecchi P, Boulouchos K. Derivation of burning velocities of premixed hydrogen/air flames at engine-relevant conditions using a single-cylinder compression machine wiht optical access. Int J Hydrogen Energy 2010;35:2566-77.
[34] Saxena P, Williams FA. Testing a small detailed chemical–kinetic mechanism for the combustion of hydrogen and carbon monoxide. Combust Flame 2006;145:316–23.
[35] Konnov AA. Remaining uncertainties in the kinetic mechanism of hydrogen combustion. Combust Flame 2008;152:507–28.

[36] Verhelst S, Sierens R. A Two-Zone Thermodynamic Model for Hydrogen-Fueled S.I. Engines, 7th COMODIA – Int. Conf. on Modeling and Diagnostics for Advanced Engine Systems, Sapporo, Japan, July 28-31 2008, paper FL1-3

[37] Ó Conaire M, Curran H, Simmie J, Pitz W, Westbrook C. A comprehensive modeling study of hydrogen oxidation. Int J Chem Kinet 2004;36:603–22.

[38] Williams FA, Grcar JF. A hypothetical burning-velocity formula for very lean hydrogen–air flames. Proc Combust Inst 2009;32:1351–7.

[39] Konnov AA. Refinement of the kinetic mechanism of hydrogen combustion. J Adv Chem Phys 2004;23:5–18.

[40] Zimont V. Gas premixed combustion at high turbulence. Turbulent flame closure combustion model. Exp Ther Fluid Sci 2000;21:179–86.

[41] Williams FA. Detailed and reduced chemistry for hydrogen autoignition. J Loss Prev Process Indust 2008;21:131–5.

[42] Ströhle J, Myhrvold T. An evaluation of detailed reaction mechanisms for hydrogen combustion under gas turbine conditions. Int J Hydrogen Energy 2007;32:125-135.

[43] Metghalchi M, Keck JC. Laminar Burning Velocity of Propane-Air Mixtures at High Temperature and Pressure, Combust Flame 1980;38:143-54.

[44] D'Errico G, Onorati A, Ellgas S, Obieglo A. Thermo-fluid dynamic simulation of a S.I. single-cylinder H2 engine and comparison with experimental data. ASME Spring Engine Technology Conference paper nr. ICES2006-1311 (Aachen, Germany, 2006).

[45] Frassoldati A, Faravelli T, Ranzi E. A wide range modeling study of NO_X formation and nitrogen chemistry in hydrogen combustion. Int J Hydrogen Energy 2006;31:2310-28.

[46] Lipatnikov A, Chomiak J. Molecular transport effects on turbulent flame propagation and structure. Prog Energy Combust Sci 2005;31:1–73.

[47] Gerke U. Numerical analysis of mixture formation and combustion in a hydrogen direct-injection internal combustion engine. PhD thesis, Swiss Federal Institute of Technology, Zurich, Switzerland.

[48] Brewster S, Bleechmore C. Dilution Strategies for Load and NOx Management in a Hydrogen Fuelled Direct Injection Engine. SAE technical paper nr 2007-01-4097.

[49] Verhelst S, Sierens R. Combustion Studies for PFI Hydrogen IC Engines. SAE technical paper nr 2007-01-3610.

[50] Combustion Technology group, Technical University of Eindhoven, http://www.combustion.tue.nl.

[51] More JJ. The Levenberg-Marquardt algorithm: implementation and theory. Proceedings of the 1977 Dundee conference on numerical analysis (Berlin, Heidelberg, New York, Tokyo) (G. A. Watson, ed.), Lecture notes in mathematics 630, Springer Verlag, 1978, pp. 105-116.

Figure and table captions

Table captions

Table 1. The database of u_l values

Table 2. Coefficients for Eq. (11)

Table 3. Coefficients for Eq. (12)

Table 4. Fitting statistics of Eq. (13) (partial fit, f=0) and Eq. (9)-(18)-(19) (full fit, f≥0) compared to fitted data and test data

Table 5. Coefficients for Eq. (18)

Table 6. Fitting statistics of previously published correlations compared to detailed kinetics results

Figure captions

Figure 1. Laminar burning velocities plotted against air-to-fuel equivalence ratio, for NTP hydrogen-air flames. Experimentally derived correlations from Liu and MacFarlane [27], Milton and Keck [28], Iijima and Takeno [29] and Koroll et al. [30]. Other experimental data from Taylor [21], Vagelopoulos et al. [22], Kwon and Faeth [23] and Verhelst et al. [24].

Figure 2. Schlieren photographs of a λ=1.25, 300 K, 5 bar hydrogen-air flame, taken in a constant volume combustion chamber (time interval 0.385 ms), illustrating the cellular nature of the flame caused by flame front instability.

Figure 3. Plot of the natural logarithm of u_l set out against the natural logarithm of the dimensionless temperature T/T_0. Various data series are shown (pressure p given in bar), spanning the entire database illustrating the generality of the proposed power relationship.

Figure 4. Comparison between the predicted laminar burning velocity values $u_{l,pred}$ using the correlation (Eqs. (11)-(13)) and the source data upon which the correlation is based (no residual gases). The ± 10% (solid lines) and ± 20% (dashed lines) are indicated.

Figure 5. Comparison between the predicted laminar burning velocity values $u_{l,pred}$ using the correlation (Eqs. (11)-(13)) and the test data (no residual gases). The ± 10% (solid lines) and ± 20% (dashed lines) are indicated.

Figure 6. Examples of test data (open symbols) generated based on the dataset (black symbols) for intermediate temperatures (A) and pressures (B). Various data series are shown, spanning the entire database.

Figure 7. Trend analysis of the correction term F(T, λ, p, f) for varying temperatures and λ=1.

Figure 8. Comparison between the predicted laminar burning velocity values $u_{l,pred}$ using the correlation (Eqs. (9)-(11)-(13)-(18)-(19)) and the source data upon which the correlation is based (with residual gases). The ± 10% (solid lines) and ± 25% (dashed lines) are indicated.

Figure 9. Comparison between the predicted laminar burning velocity values $u_{l,pred}$ using the correlation (Eqs. (9)-(11)-(13)-(18)-(19)) and the test data (with residual gases). The ± 10% (solid lines) and ± 25% (dashed lines) are indicated.

Figure 10. Comparison between the predicted laminar burning velocity values $u_{l,pred}$ using the correlation (Eqs. (9)-(11)-(13)-(18)-(19)) and the entire dataset (fitted and test data). The ± 10% (solid lines) and ± 25% (dashed lines) are indicated.

Figure 11. Comparison between the laminar burning velocity values using previously published correlations (u_l calculated) to the values obtained using the present chemical kinetic computations (u_l from detailed kinetics). The ± 10% (solid lines) and ± 20% (dashed lines) are indicated.

Figure 12. Comparison of the calculated burning velocities for 5 combinations of pressure and temperature, at 3 air-to-fuel equivalence ratios. Burning velocities calculated with the correlations of Verhelst et al. [20,24] ("Verhelst"), Knop et al. [11] ("IFP"), Gerke et al. [32] (on the basis of their experimental results – "ETH exp" and of chemical kinetics – "ETH kin. corr."), D'Errico et al. [7] ("Milano"), and Eq. (13). Results from the detailed kinetics also shown.

Figure 13. Comparison of the calculated correction term as a function of residual gas content, for 3 combinations of pressure and temperature, for stoichiometric mixtures. Calculations done with the correlations of Verhelst et al. [19,24] (respectively "Verhelst kin." and "Verhelst expt.") and Eq. (19). Results from the detailed kinetics also shown.

Figure 14. Comparison of the calculated correction term as a function of residual gas content, for 3 combinations of pressure and temperature, for an air-to-fuel equivalence ratio λ=2. Calculations done with the correlations of Verhelst et al. [19,24] (respectively "Verhelst kin." and "Verhelst expt.") and Eq. (19). Results from the detailed kinetics also shown.

Figure1

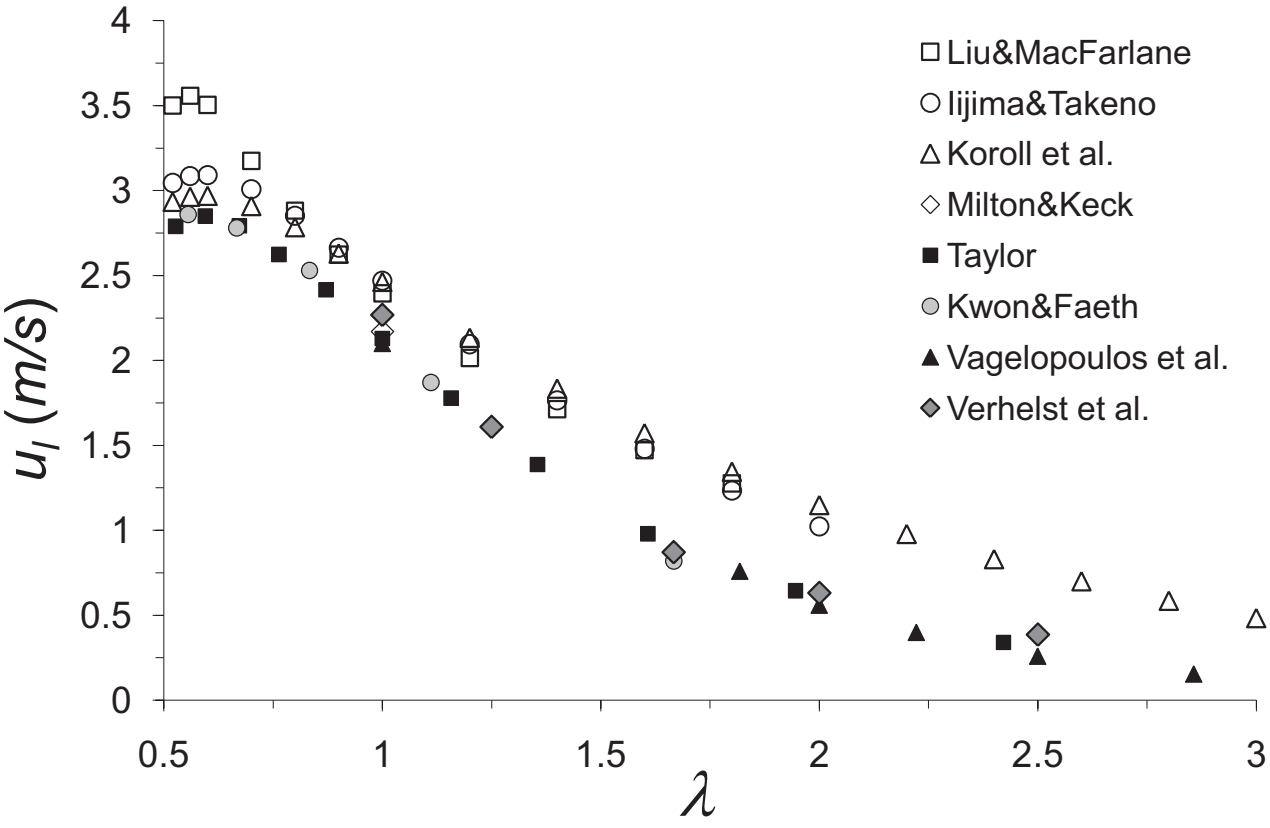
4
3.5
3
2.5
2
1.5
1
0.5
0
0.5
1
1.5
2
2.5
3
u_l (m/s)
λ
Liu&MacFarlane
Iijima&Takeno
Koroll et al.
Milton&Keck
Taylor
Kwon&Faeth
Vagelopoulos et al.
Verhelst et al.

Figure2

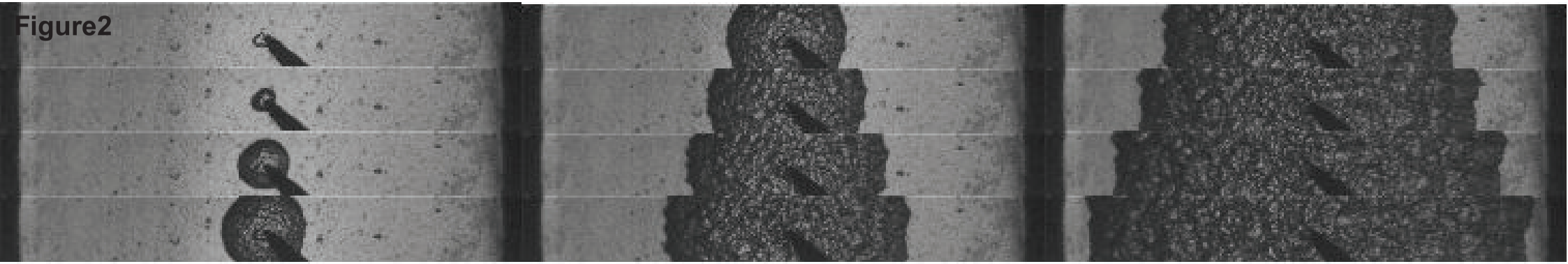

Figure3

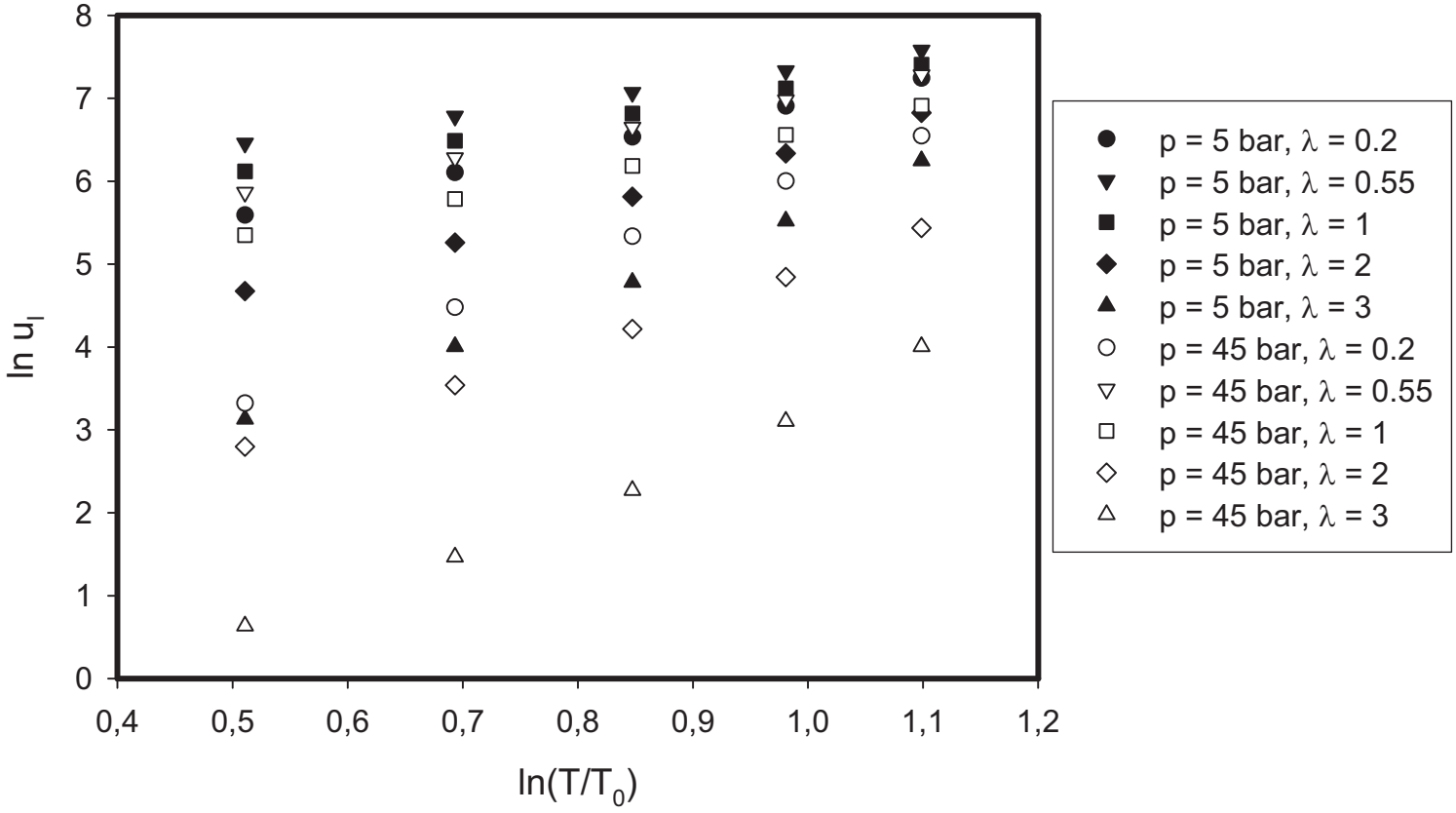
8
7
6
5
4
3
2
1
0
ln u_l
0,4
0,5
0,6
0,7
0,8
0,9
1,0
1,1
1,2
ln(T/T_0)
p = 5 bar, λ = 0.2
p = 5 bar, λ = 0.55
p = 5 bar, λ = 1
p = 5 bar, λ = 2
p = 5 bar, λ = 3
p = 45 bar, λ = 0.2
p = 45 bar, λ = 0.55
p = 45 bar, λ = 1
p = 45 bar, λ = 2
p = 45 bar, λ = 3

Figure4

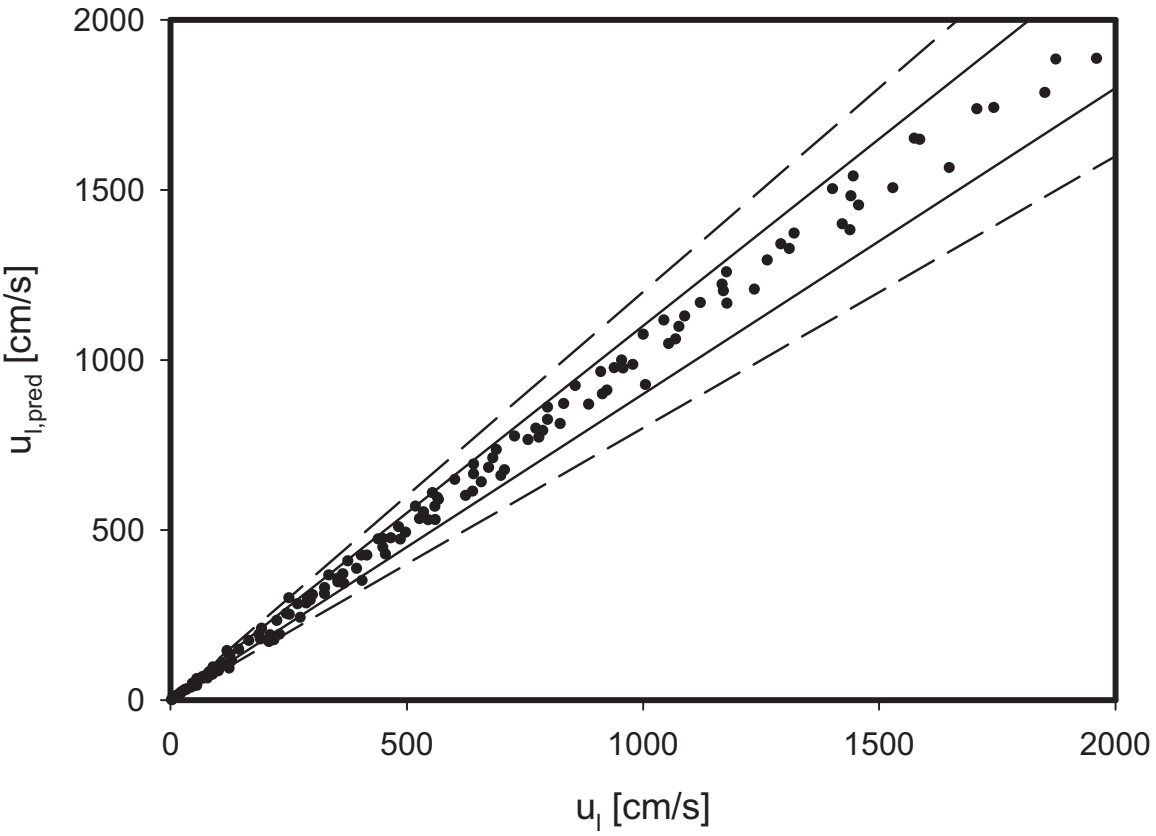

Figure5

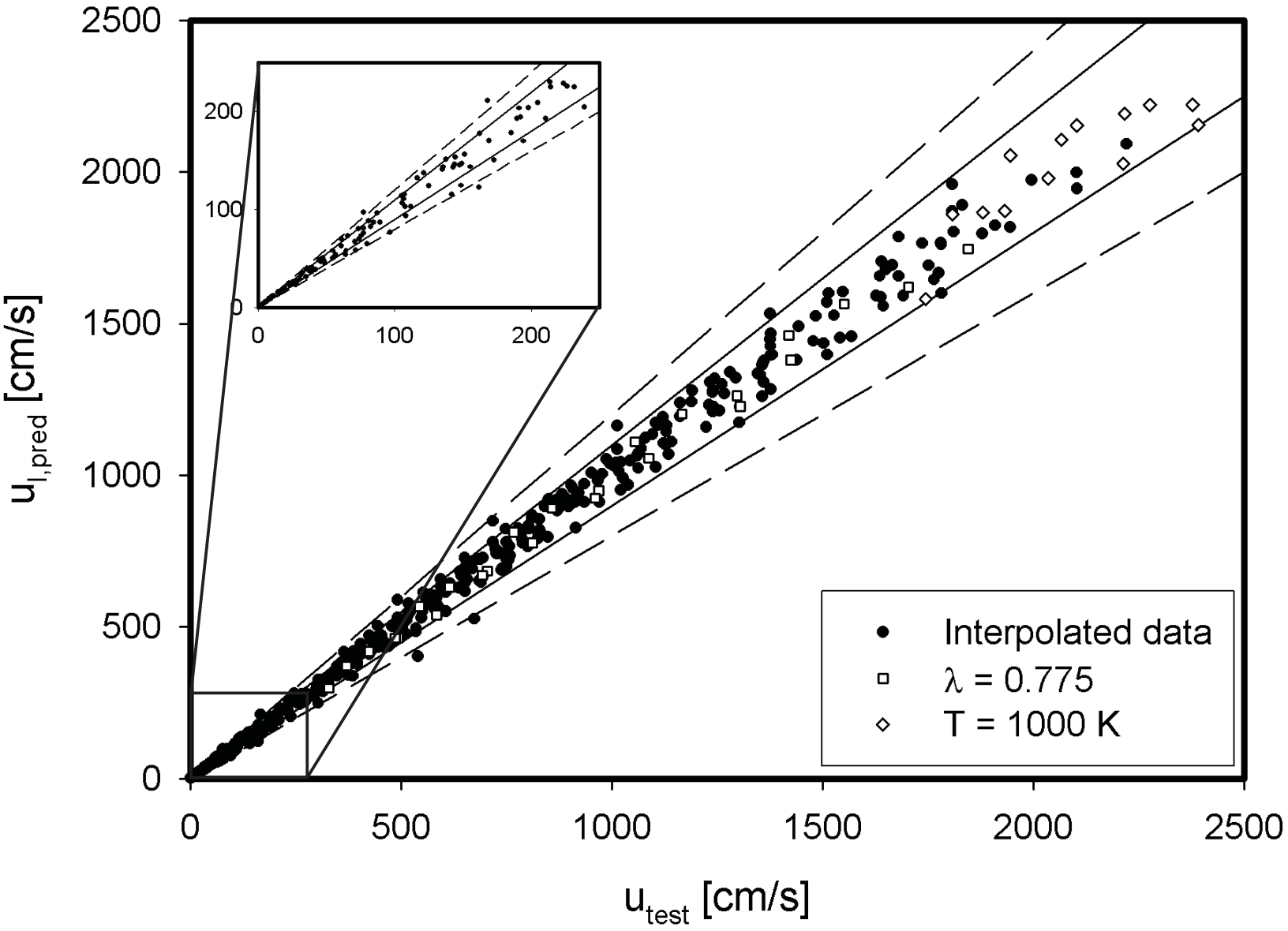
2500
2000
1500
1000
500
0
0
500
1000
1500
2000
2500
$u_{l,pred}$ [cm/s]
u_{test} [cm/s]
200
100
0
0
100
200
Interpolated data
λ = 0.775
T = 1000 K

Figure6

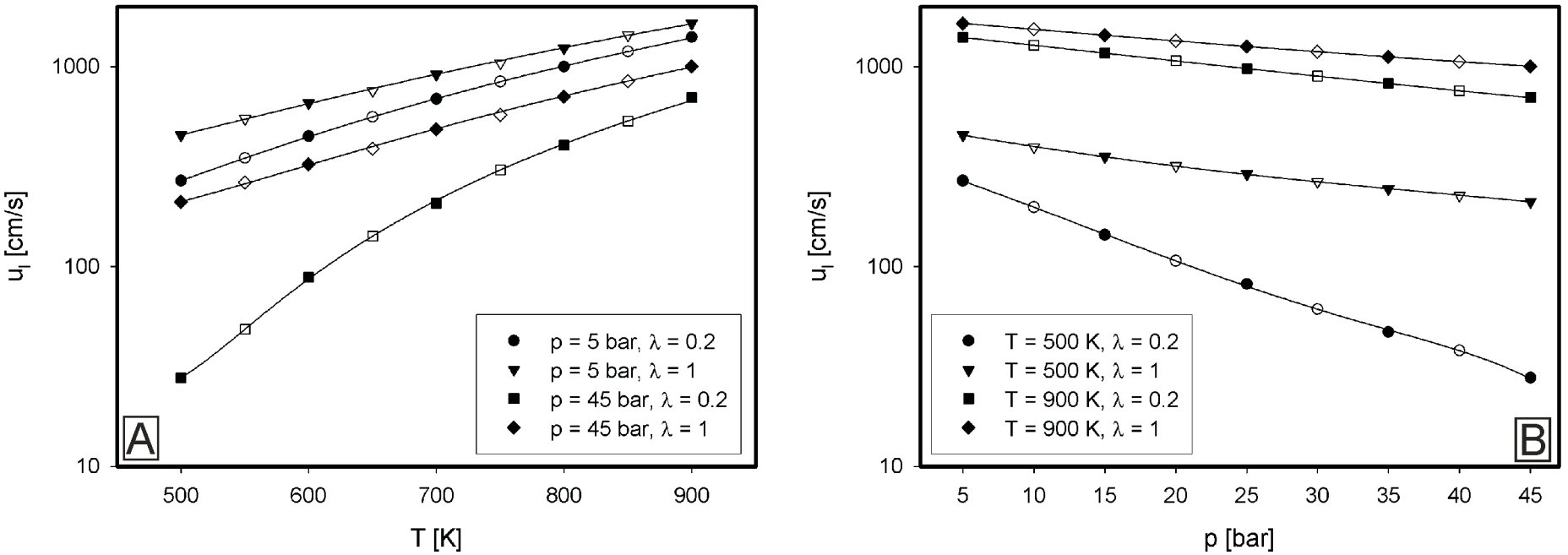
1000
100
10
u_l [cm/s]
500
600
700
800
900
T [K]
A
p = 5 bar, λ = 0.2
p = 5 bar, λ = 1
p = 45 bar, λ = 0.2
p = 45 bar, λ = 1
1000
100
10
u_l [cm/s]
5
10
15
20
25
30
35
40
45
p [bar]
B
T = 500 K, λ = 0.2
T = 500 K, λ = 1
T = 900 K, λ = 0.2
T = 900 K, λ = 1

Figure7

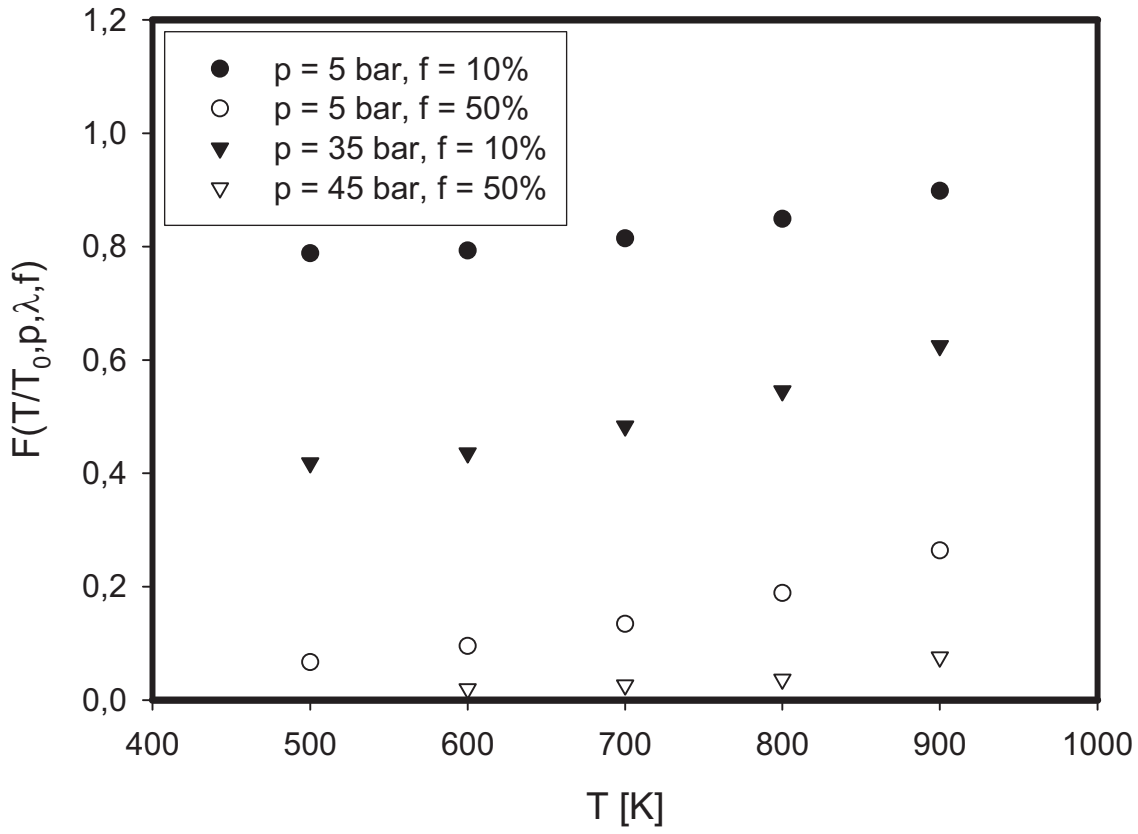
1,2
1,0
0,8
0,6
0,4
0,2
0,0
400
500
600
700
800
900
1000
T [K]
F(T/T0,p,λ,f)
p = 5 bar, f = 10%
p = 5 bar, f = 50%
p = 35 bar, f = 10%
p = 45 bar, f = 50%

Figure8

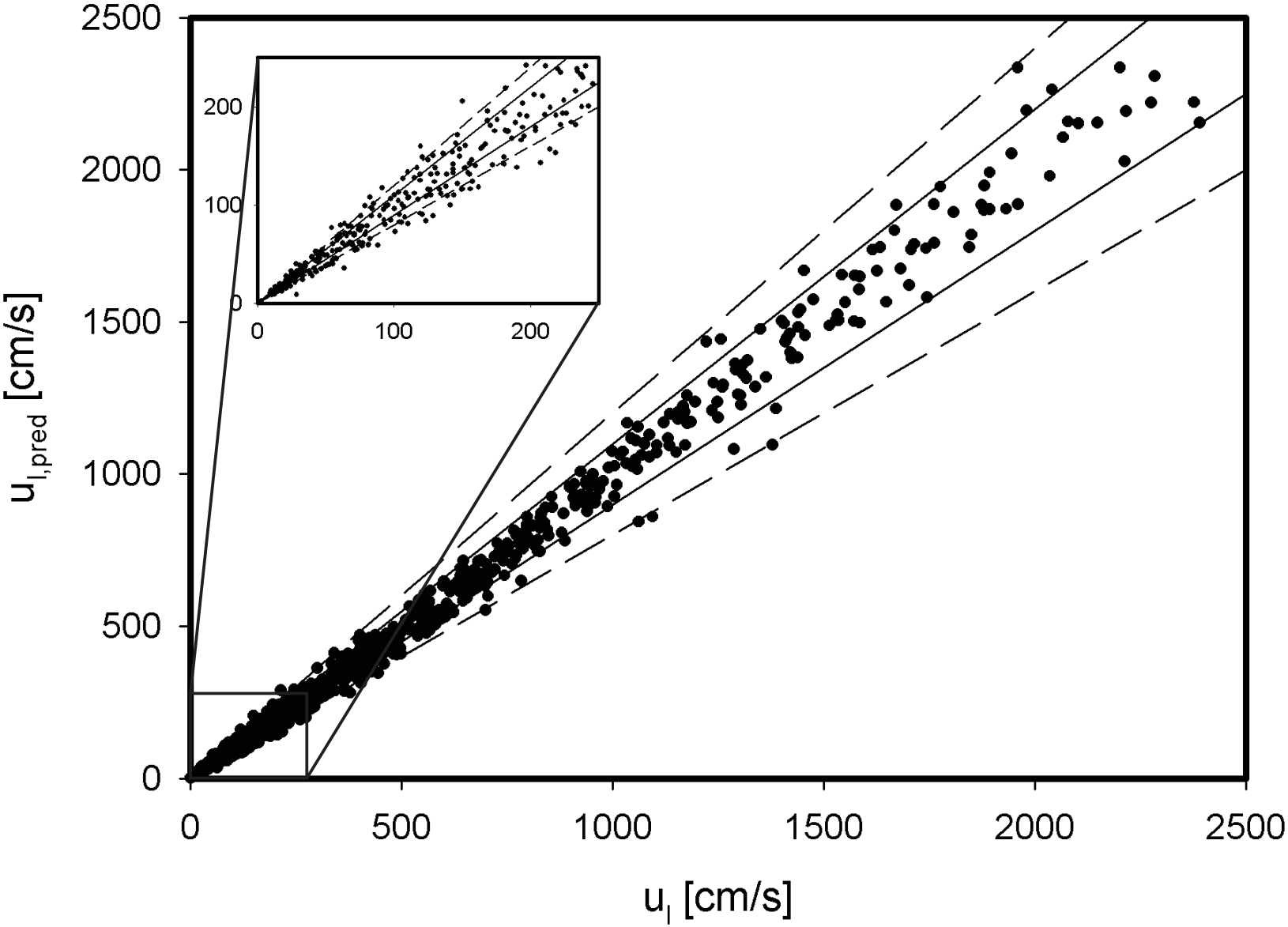
2500
2000
1500
1000
500
0
0
500
1000
1500
2000
2500
$u_{l,pred}$ [cm/s]
u_l [cm/s]
200
100
0
0
100
200

Figure9

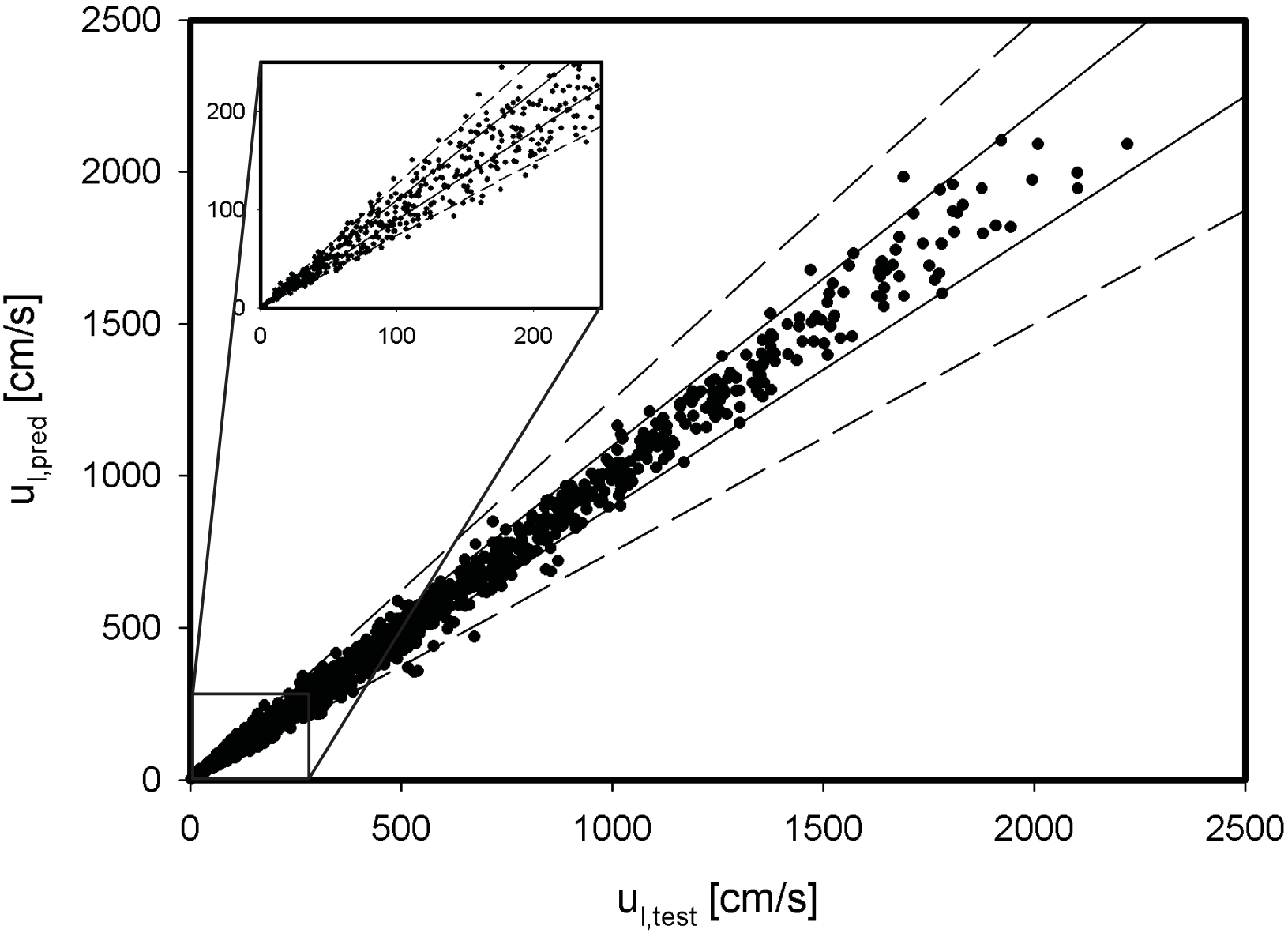
2500
2000
1500
1000
500
0
0
500
1000
1500
2000
2500
$u_{l,pred}$ [cm/s]
$u_{l,test}$ [cm/s]
200
100
0
0
100
200

Figure10

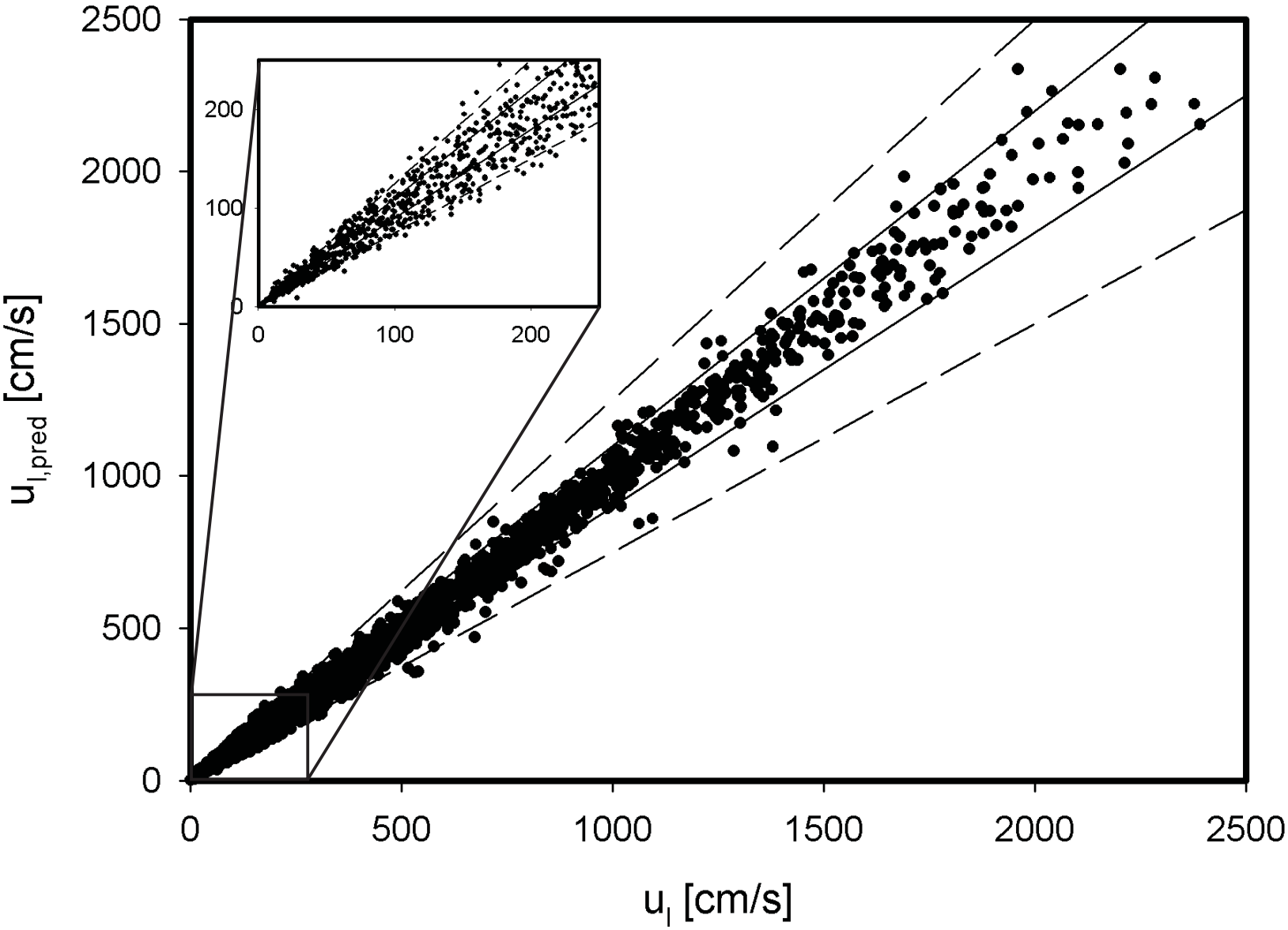
2500
2000
1500
1000
500
0
0
500
1000
1500
2000
2500
$u_{l,pred}$ [cm/s]
u_l [cm/s]
200
100
0
0
100
200

Figure11

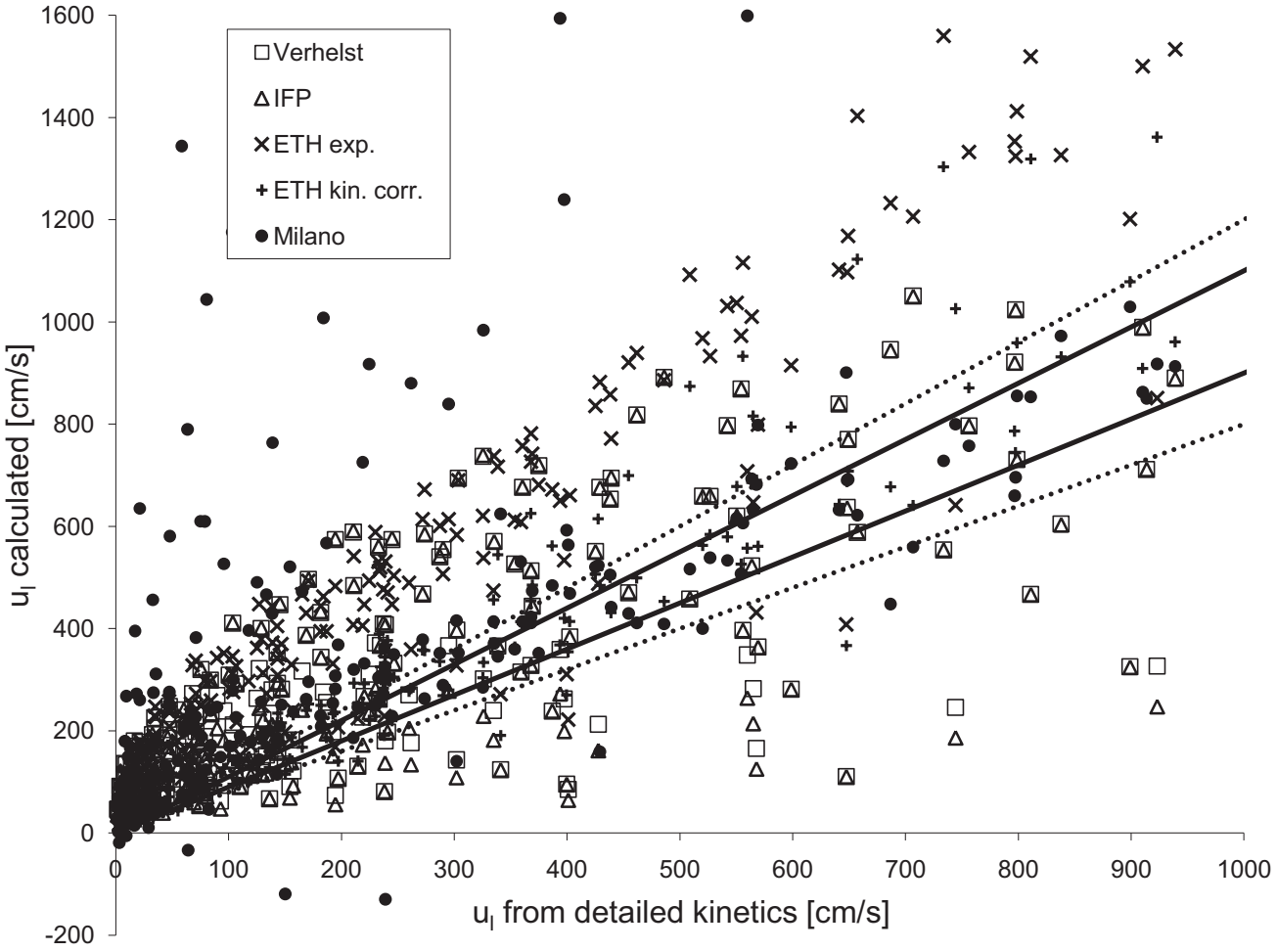
Verhelst
IFP
ETH exp.
ETH kin. corr.
Milano
1600
1400
1200
1000
800
600
400
200
0
-200
0
100
200
300
400
500
600
700
800
900
1000
u_l calculated [cm/s]
u_l from detailed kinetics [cm/s]

Figure12

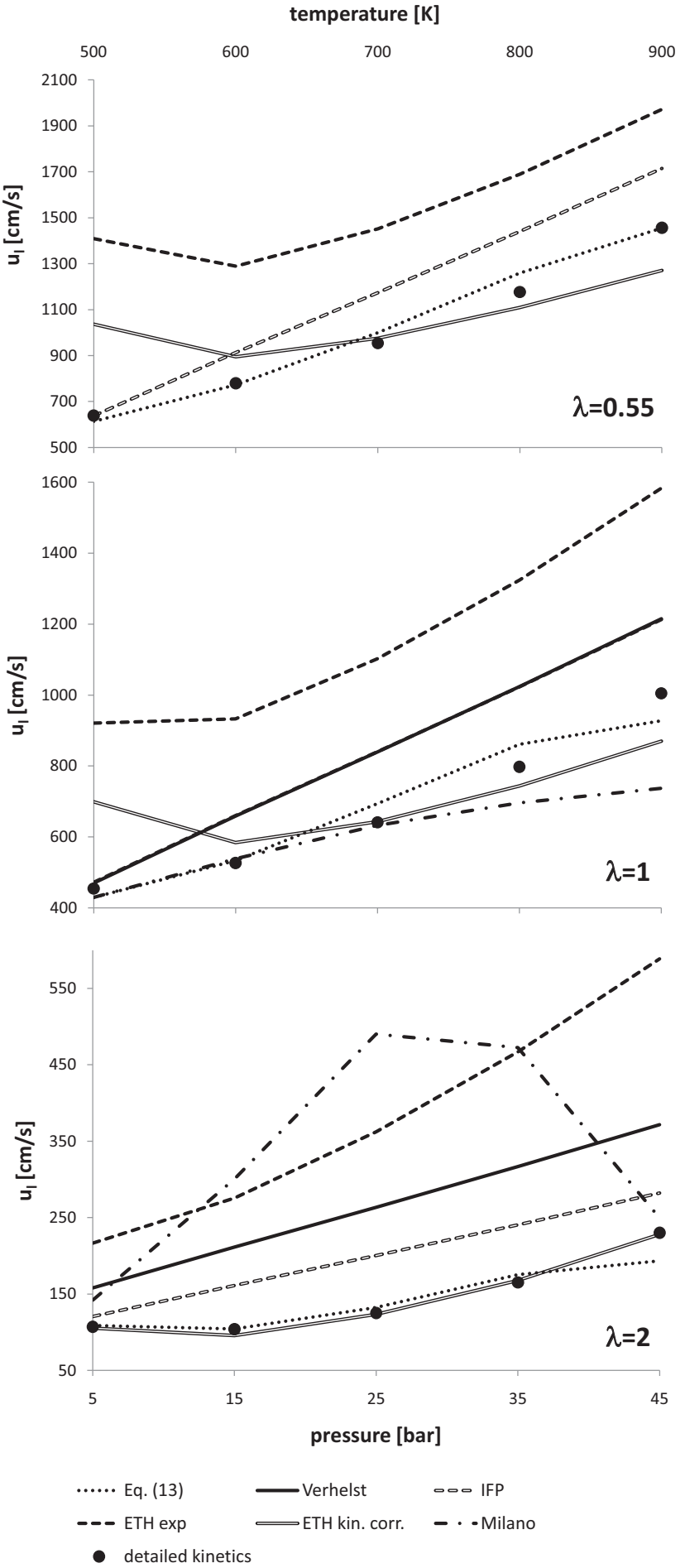
temperature [K]
500
600
700
800
900
2100
1900
1700
1500
1300
1100
900
700
500
u_l [cm/s]
λ=0.55
1600
1400
1200
1000
800
600
400
u_l [cm/s]
λ=1
550
450
350
250
150
50
u_l [cm/s]
λ=2
5
15
25
35
45
pressure [bar]
Eq. (13)
Verhelst
IFP
ETH exp
ETH kin. corr.
Milano
detailed kinetics

Figure13

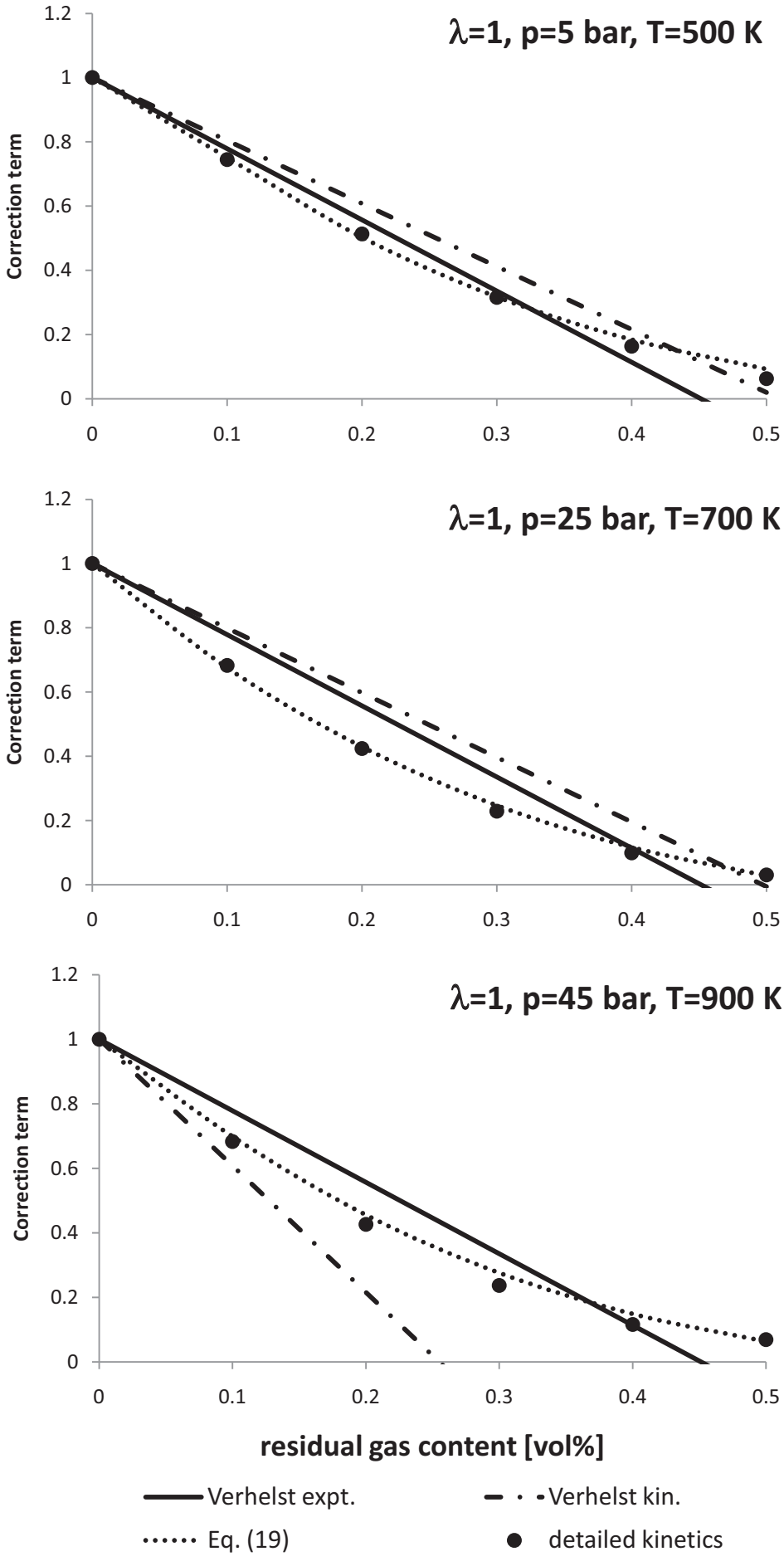
λ=1, p=5 bar, T=500 K
λ=1, p=25 bar, T=700 K
λ=1, p=45 bar, T=900 K
Correction term
residual gas content [vol%]
Verhelst expt.
Verhelst kin.
Eq. (19)
detailed kinetics

Figure14

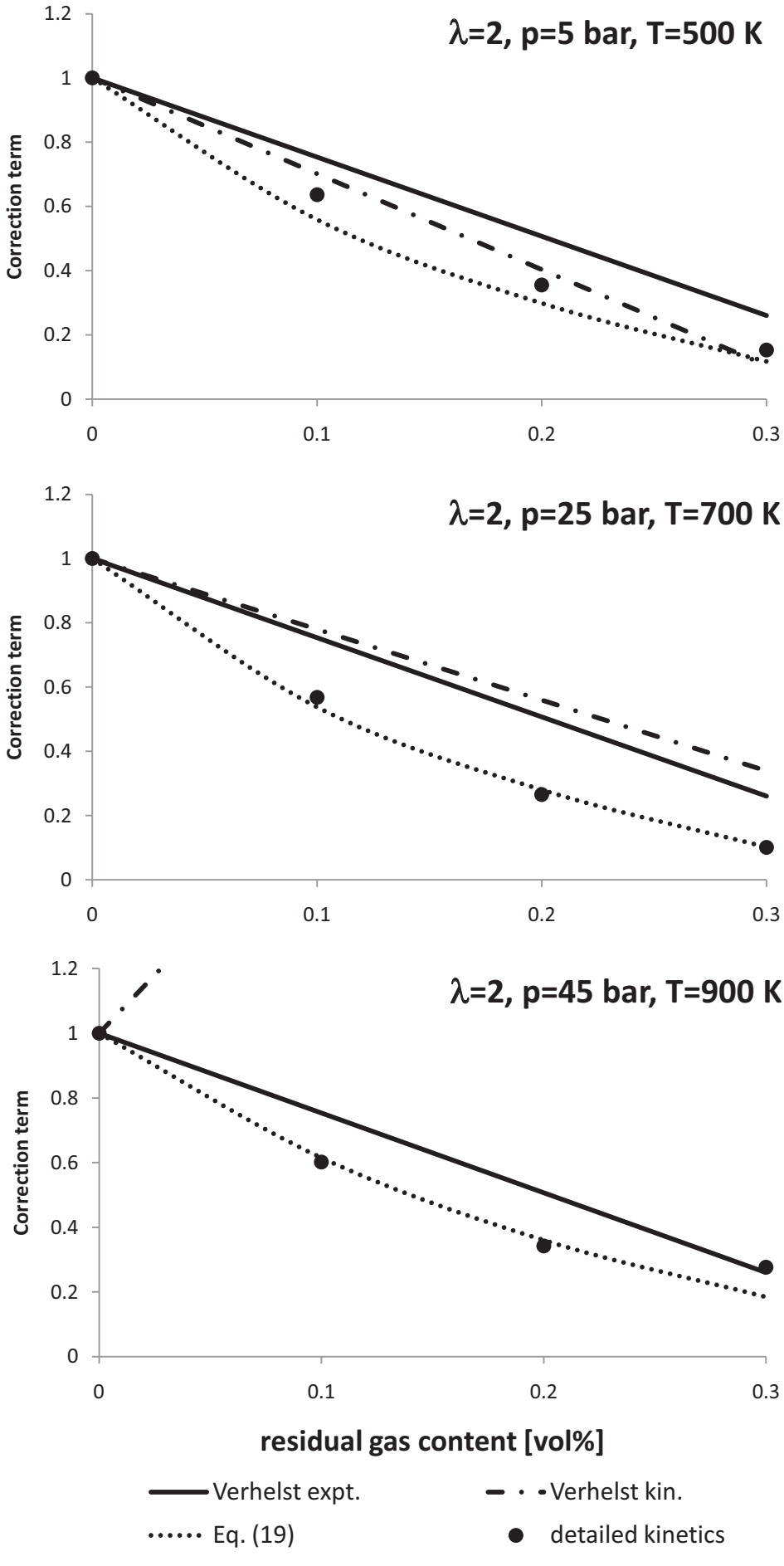
λ=2, p=5 bar, T=500 K
λ=2, p=25 bar, T=700 K
λ=2, p=45 bar, T=900 K
Correction term
1.2
1
0.8
0.6
0.4
0.2
0
0
0.1
0.2
0.3
residual gas content [vol%]
Verhelst expt.
Verhelst kin.
Eq. (19)
detailed kinetics

Table1

Table 1: The database of u_l values

p\T	500 K	600 K	700 K	800 K	900 K
5	**X**	X	X	X	X
15	X	**X**	X	X	X
25	X	X	**X**	X	X
35	X	X	X	**X**	X
45	X	X	X	X	**X**

λ\f	0	0.1	0.2	0.3	0.4	0.5
0.2	X	X	-	-	-	-
0.38	X	X	X	X	-	-
0.55	X	X	X	X	X	X
0.775	X	X	X	X	X	X
1	X	X	X	X	X	X
2	X	X	X	X	X	X
3	X	X	X	X	X	X

Table2

Table 2: coefficients for Eq. (11)

a_1	0.584069
a_2	1.097884
a_3	-3.683272 e-2
a_4	2.454259 e-2
a_5	0.104381
a_6	-4.119350 e-4
a_7	7.621143 e-3
a_8	7.62759 e-4
a_9	-4.498380 e-4
a_{10}	0.331465
a_{11}	2.165434 e-2

Table3

Table 3: coefficients for Eq. (12)

b_1	7.505661
b_2	-1.903711
b_3	5.380840 e-2
b_4	-3.936929 e-2
b_5	1.896873 e-2
b_6	5.964680 e-4
b_7	-3.010525 e-2
b_8	-3.431092 e-4
b_9	9.023031 e-4
b_{10}	-1.556492 e-5
b_{11}	8.452404 e-4
b_{12}	-0.478534
b_{13}	-3.105883 e-2

Table4

Table 4. Fitting statistics of Eq. (13) (partial fit, f=0) and Eq. (9)-(18)-(19) (full fit, f≥0) compared to fitted data and test data

	$u_{l,pred}$ (Eq. (13))	$u_{l,pred}$ (Eq. (13)): test data	$u_{l,pred}$ (Eq. (13)-(18)-(19))	$u_{l,pred}$ (Eq. (13)-(18)-(19)): test data
Average rel. residual	0.007 %	-0.81%	-4.3%	-1.5%
Average abs. rel. residual	5.67%	4.78%	10.1%	9.3 %
Maximum residual	21.7%	25.9%	41%	48.4%
Minimum residual	-24%	-24.2%	-44%	-34.1%
Data within ±10%	85.3%	94.3%	73.1%	84%
Data within ±20%	96.6%	99.1%	87.8%	89%
Data within ±25%	100%	99.7%	94.5%	94%

Table5

Table 5: coefficients for Eq. (18)

c_1	1.782191
c_2	-1.945813E-01
c_3	-4.071734E-03
c_4	-4.987061E-01
c_5	-4.347767
c_6	8.576177E-05
c_7	4.490150E-02
c_8	7.878902E-02
c_9	4.243647
c_{10}	-2.052509E-03
c_{11}	3.724404E-03
c_{12}	-2.114637E-01
c_{13}	-2.224738E-01
c_{14}	4.624703E-02
c_{15}	2.116186E-01
c_{16}	-2.098941
c_{17}	7.029643E-02
c_{18}	1.334951
c_{19}	4.861730E-04
c_{20}	-1.915344E-02
c_{21}	6.146191E-01

Table6

Table 6. Fitting statistics of previously published correlations compared to detailed kinetics results

	Verhelst	IFP	ETH exp.	ETH kin. corr.	Milano
Average rel. residual	225.9	170.7	275.8	42.7	246.6
Average abs. rel. residual	243.6	192.0	277.5	46.9	268.2
Maximum residual	2815.4	2128.6	2327.3	270.3	2889.8
Minimum residual	-82.9	-83.9	-44.7	-44.1	-714.6
Data within ±10%	6.5	6.1	1.7	17.0	12.6
Data within ±20%	12.2	13.3	3.7	31.0	22.1
Data within ±25%	15.6	17.3	4.8	35.7	25.9